Nsr1, a nitrogen source-regulated microprotein, confers an alternative mechanism of G1/S transcriptional activation in budding yeast

Sylvain Tollis[1,*,†], Jaspal Singh[2,†] , Yogitha Thattikota[1,‡], Xiaojing Tang[2], Susan Moore[1], Deborah Blake[1], Jasmin Coulombe-Huntington[1], Eric Bonneil[1], Catherine A. Royer[3], Pierre Thibault[1] and Mike Tyers[1,*]

[1] Institute for Research in Immunology and Cancer, University of Montréal, Montréal, Quebec, Canada

[2] Lunenfeld-Tanenbaum Research Institute, Mount Sinai Hospital, Toronto, Ontario, Canada

[3] Department of Biological Sciences, Rensselaer Polytechnic Institute, Troy, NY, USA

[†] equal contribution to this work

[‡] Present address: Montreal Neurological Institute, McGill University, Montréal, Quebec, Canada; Department of Neurology and Neurosurgery, McGill University, Montreal, Quebec, Canada

* To whom correspondence should be addressed: sylvain.tollis@umontreal.ca; md.tyers@umontreal.ca

keywords: Saccharomyces cerevisiae, genetic screen, G1/S transcription, Start, transcription factor, nutrient limitation, microprotein, evolution, quantitative microscopy

running title: A microprotein activates G1/S transcription under nitrogen limitation

Abstract

Commitment to cell division at the end of G1 phase, termed Start in the budding yeast *Saccharomyces cerevisiae*, is strongly influenced by nutrient availability. To identify new dominant activators of Start that might operate under different nutrient conditions, we screened a genome-wide ORF overexpression library for genes that bypass a Start arrest caused by absence of the G1 cyclin Cln3 and the transcriptional activator Bck2. We recovered a hypothetical gene *YLR053c*, renamed *NSR1* for Nitrogen-responsive Start Regulator 1, which encodes a poorly characterized 108 amino acid microprotein. Endogenous Nsr1 was nuclear-localized, restricted to poor nitrogen conditions, induced upon mTORC1 inhibition, and cell cycle-regulated with a peak at Start. *NSR1* interacted genetically with *SWI4* and *SWI6*, which encode the master G1/S transcription factor complex SBF. Correspondingly, Nsr1 physically interacted with Swi4 and Swi6 and was localized to G1/S promoter DNA. Nsr1 exhibited inherent transactivation activity and fusion of Nsr1 to the SBF inhibitor Whi5 was sufficient to suppress other Start defects. Nsr1 appears to be a recently evolved microprotein that rewires the G1/S transcriptional machinery under poor nutrient conditions.

Author Summary

Unicellular microorganisms must adapt to ever-changing nutrient conditions and hence must adjust cell growth and proliferation to maximize fitness. In the budding yeast *Saccharomyces cerevisiae*, commitment to cell division, termed Start, is heavily influenced by nutrient availability. The mechanisms of Start activation under conditions of nutrient limitation are less well characterized than under nutrient excess. To identify potential new Start regulators specific to poor nutrient environments, we screened for genes able to bypass a genetic Start arrest caused by loss of the G1 cyclin Cln3 and the transcriptional activator Bck2. This screen uncovered *YLR053c*, which we renamed *NSR1* for Nitrogen-responsive Start Regulator. Sequence analysis across yeast species indicated that Nsr1 is a recently-evolved microprotein. We showed that *NSR1* is nutrient- and cell cycle-regulated, and directly binds the main G1/S transcription factor complex SBF. We demonstrated that Nsr1 has an intrinsic trans-activation activity and provided genetic evidence to suggest that Nsr1 can bypass the requirement for normal Cln3-dependent

activation of SBF. These results uncover a new mechanism of Start activation and demonstrate how microproteins can rapidly emerge to rewire fundamental cellular processes.

Introduction

All organisms have evolved adaptive regulatory mechanisms to optimize fitness in the face of ever-changing environmental conditions. This ability to adapt is particularly important for unicellular organisms which lack the capacity to establish the internal homeostatic environment of metazoan species. In the budding yeast *Saccharomyces cerevisiae*, different carbon and nitrogen sources can dramatically affect the rates of cell growth and division, as well as developmental programs (1). Yeast cells commit to division at the end of G1 phase, an event referred to as Start (2, 3). In order to pass Start, cells must grow to a characteristic critical size that constrains the overall size distribution of an asynchronous population of cells. The size threshold dynamically adjusts to changing nutrient availability thereby optimizing competitive fitness (3). How nutrient conditions modulate the growth and division machinery at the molecular level is still largely unknown.

Start initiates a complex G1/S transcriptional program of ~200 genes that encode proteins necessary for bud emergence, DNA replication, spindle body duplication and other processes. This program is controlled by two transcription factor complexes, SBF (Swi4/6 Cell Cycle Box binding factor) and MBF (MluI Cell Cycle Box binding factor), each comprised of related DNA-binding proteins, Swi4 and Mbp1 respectively, coupled to a common regulatory subunit Swi6 (4, 5). Individually Swi4 and Mbp1 are not essential but a double *swi4Δ mbp1Δ* mutant is inviable (6), consistent with the significant overlap between SBF and MBF binding sites in G1/S promoters (7-10). In pre-Start cells that have not achieved the critical cell size, SBF is inhibited by the Whi5 transcriptional repressor(11-13). At Start, the G1 cyclin (Cln)-Cdc28 protein kinases phosphorylate both SBF and Whi5 to disrupt the SBF-Whi5 interaction and trigger Whi5 nuclear export (12-14). The upstream G1 cyclin Cln3 is thought to initiate a positive feedback loop in which SBF-dependent expression of *CLN1/2* further amplifies (Cln)-Cdc28 activity and thus SBF activation (15, 16). The expression of Cln3 itself does not rely on the SBF-dependent positive feedback (17). Although *CLN3* was isolated as a potent dose-dependent activator of Start(18), the

size-dependent mechanism whereby Cln3-Cdc28 initiates the SBF positive feedback loop remains uncertain (19, 20). *CLN3* is essential only in the absence of other parallel activators of Start, most notably *BCK2*, which encodes a general transcriptional activator (21, 22).

Connections between the main yeast nutrient signalling conduits, the cell size threshold and Start have been established. Activation of the protein kinase A (PKA) pathway by glucose represses *CLN1* and other G1/S transcripts, which may increase the cell size threshold in rich nutrients (23, 24). The TOR signalling network, which controls many aspects of cell growth including the rate of ribosome biogenesis, has been linked to the size threshold (11, 25-27). The TORC1 complex phosphorylates and activates the effector kinase Sch9 and the master transcription factor Sfp1 to activate ribosomal protein (RP) and ribosome biogenesis (Ribi) genes (25, 26, 28). Deletion of either *SFP1* or *SCH9* abrogates the carbon source-dependent control of cell size (25). The Rim15 kinase, which is active under respiratory growth conditions in poor carbon sources, may suppress the Cdc55 phosphatase that dephosphorylates Whi5, and thereby contribute to Whi5 inactivation even when Cln3 activity is low (29). Poor nutrient conditions also increase the expression of the G1/S transcription factors and thereby activate Start at a smaller cell size (30). Notably though, a *cln3Δ bck2Δ whi5Δ* triple mutant is completely viable and still responds to nutrient cues, suggesting that nutrient regulation of Start may be partly independent of the Cln3-Bck2-Whi5-SBF axis (12, 25).

To identify nutrient-dependent activators of Start that might act in parallel to the central Cln3-Bck2-Whi5 pathway, we screened for dosage suppressors of the lethal *cln3Δ bck2Δ* Start arrest phenotype (12, 13, 31, 32). This screen identified *YLR053c*, a poorly characterized hypothetical gene that encodes a recently evolved 108 amino acid microprotein, which we renamed *NSR1* for Nitrogen-responsive Start Regulator 1. Nsr1 protein was only observed in poor nitrogen conditions and was cell cycle-regulated with peak nuclear localization at Start. Nsr1 genetically and physically interacted with SBF, and caused a small size phenotype when overexpressed in wild type cells. Nsr1 exhibited intrinsic trans-activation activity and direct fusion of Nsr1 to Whi5 was sufficient to reduce cell size in rich carbon sources and rescue the *cln3Δ bck2Δ* lethality. These results demonstrate that the recently evolved Nsr1 microprotein allows cells to adapt to

poor nutrient conditions by rewiring the Start transcriptional machinery.

Results

A genome-wide screen identifies overexpression of YLR053c as a rescue of cln3Δ bck2Δ lethality

We constructed a *cln3Δ bck2Δ whi5::GAL1-WHI5* strain that is viable in glucose medium but not in galactose due to conditional *WHI5* expression (12, 13). We used the SGA methodology to cross this query strain to an array of 5280 *GAL1-GST-ORF* strains (33-35) and assessed the growth of the resulting array in galactose (Figure 1A, B). Three replicates of the screen identified 12 genes that reproducibly rescued the *cln3Δ bck2Δ* lethal Start arrest (Table 1). These genes included the G1 cyclins *CLN1* and *CLN3* but not other known Start activators such as *CLN2*, *BCK2*, *SWI4* and *SWI6*, possibly due to the *WHI5* overexpression and/or overexpression toxicity of particular genes. We recovered 10 genes not known to be Start regulators such as *YEA4*, which encodes a uridine diphosphate-N-acetylglucosamine transporter. Notably, the short hypothetical ORF *YLR053c* restored *cln3Δ bck2Δ* growth to the same extent as *CLN3*, as assessed by direct transformation of the query strain with *GAL1-YLR053c* and *GAL1-CLN3* constructs (Figure 1C).

YLR053c encodes a 108 residue microprotein that is only poorly characterized. Microproteins are often encoded by newly evolved proto-genes that are thought to form a genetic reservoir that fuels adaptive evolution (36). To gain insight into the *YLR053c* locus evolution, we aligned the Ylr053c protein sequence from *S. cerevisiae* with predicted orthologs from other yeast species (Figure 1D, E). The *YLR053c* locus appears to have evolved relatively rapidly within the Saccharomyces sensu stricto group, with a dN/dS ratio in the 98th, 79th and 90th percentile in *S. mikatae*, *S. bayanus* and *S. castellii*, respectively as compared with *S. cerevisiae* (Figure S1A). In comparison, the evolution of other core Start regulators was closer to the genome median, with dN/dS ratios in the 74th, 77th and 58th percentile for *WHI5*, 69th, 75th and 31st percentile for *SWI4*, and 82nd, 51st and 43rd percentile for *SWI6*. A 17 amino acid sequence at the Ylr053c C-terminal region was conserved even in more distant yeasts such as *K. waltii* (Figure 1E). From this point forward, we refer to *YLR053c* as *NSR1* for reasons described below.

Nsr1 is induced by rapamycin and nitrogen limitation

To understand the function of Nsr1 we first sought to characterize its endogenous expression. We performed scanning Number and Brightness (sN&B) confocal microscopy to localize and quantify Nsr1 fused with GFPmut3 at the subcellular scale in live wild-type (WT) cells under a range of conditions (30, 37). GFPmut3, a monomeric fast-folding GFP mutant (38), will be referred to here as GFP for brevity. Nsr1-GFP was not detected in cells grown on either SC+2% glucose or SC+2% raffinose medium (Figure 2A), consistent with previous analysis of *YLR053/NSR1* mRNA levels (39). In contrast, Nsr1-GFP was readily detected in the nucleus of cells grown overnight to mid log-phase in nitrogen-limited YNB pro glu medium (Figure 2A). This result was consistent with genome-wide transcriptome analysis under various nutrient conditions (40). Inhibition of TORC1 with 100nM rapamycin rapidly and transiently induced Nsr1-GFP expression and nuclear localization in rich SC+2% glucose medium (Figure 2A; Figure S1B). These expression patterns were confirmed with an independent Nsr1-wtGFP fusion protein (Figure S1C). Hyperosmotic stress, oxidative stress and DNA damage did not induce Nsr1 expression in SC+2% glucose medium (Figure S1D). Immunoblot analysis of strains bearing a MYC epitope-tagged version of Nsr1 in different carbon and nitrogen sources, as well as in rapamycin-treated and saturated cultures, confirmed the specific expression of Nsr1 only under conditions of nitrogen limitation or TORC1 inhibition (Figure 2B). In accord with its genetic role at Start and expression pattern, we therefore renamed the gene *NSR1* for Nitrogen-responsive Start Regulator.

Nsr1 abundance peaks at the G1/S transition

We quantified Nsr1 level in asynchronous populations of live cells grown in nitrogen-limited YNB pro glu medium with our custom sN&B analysis software (30). Single cell-averaged Nsr1 levels were between 5 and 20 nM. Higher levels were observed in cells close to the typical critical size at the end of G1 phase, where the predominant nuclear Nsr1-GFP signal corresponded to 60-80 nM (Figure 2C). These Nsr1 nuclear levels at Start were comparable to Swi4 (50-100 nM), Whi5 (100-120 nM) and Swi6 (130-170 nM) levels determined previously by the same method (30). We further confirmed Nsr1 expression and nuclear localization in large unbudded and small budded cells in images acquired by standard confocal microscopy (Figure 2D). The cell cycle-regulated expression pattern of Nsr1 protein suggested that it plays a role at Start, consistent with the

suppression of the *cln3Δ bck2Δ* arrest by *NSR1* overexpression.

Overexpressed NSR1 genetically interacts with SBF

To investigate the molecular mechanism by which Nsr1 promotes Start, we examined genetic interactions of *NSR1* with the main known Start regulators. Overexpression of *NSR1* from the *GAL1* promoter, either integrated at the *NSR1* locus or from a multi-copy plasmid, caused a pronounced small size phenotype, in agreement with its putative role as a Start activator (Figure 3A, B). To interrogate the genetic requirements for this size phenotype, we transformed deletion mutants of known Start regulators with a *GAL1-NSR1* multi-copy plasmid and examined cell size epistasis. Strikingly, *NSR1* overexpression almost entirely rescued the large size phenotype of a *cln3Δ* mutant and partially rescued the large size of a *bck2Δ* mutant (Figure 3B). A *whi5Δ* mutant was epistatic to *NSR1* overexpression while a *nsr1Δ* deletion did not exacerbate the larger size caused by *WHI5* overexpression and only modestly increased the size of a *whi5Δ* mutant (Figure 3C). Notably, the small size caused by *NSR1* overexpression was abrogated in *swi6Δ* and *swi4Δ* mutant strains (Figure 3D). This requirement for *SWI4* function was further demonstrated with a temperature-sensitive *swi4* strain grown at the semi-permissive temperature of 30°C (Figure 3E). In contrast to its overexpression, deletion of *NSR1* did not detectably affect overall growth rate or cell size in any growth media tested (Figure S2A-D). Moreover, in competitive growth experiments, *nsr1Δ* and WT cells had indistinguishable fitness (Figure S2E). Taken together, these results suggested that overexpression of Nsr1 promotes small cell size upstream of Whi5-inhibited SBF independently of Cln3 and Bck2.

Endogenous Nsr1 interacts with SBF in vivo and in vitro

We next sought to identify Nsr1 protein interactors in physiological conditions. We performed immunoaffinity purification on lysates from an endogenously tagged Nsr1^{13MYC} strain grown in nitrogen-limited YNB-pro-glu medium. Analysis of the samples by mass spectrometry using stringent thresholds (Methods) identified multiple peptides (Table S3) in both Nsr1^{13MYC} cells and untagged wild-type strains, from which individual proteins were identified with high confidence (> 2 unique peptides, false discovery rate < 1%, Table S4). Comparison between Nsr1^{13MYC} and

untagged negative control strains identified 47 proteins in the Nsr1^{13MYC} sample specifically (Table S2). Nsr1 was represented by 7 peptides (48% coverage), Swi4 by 5 peptides, and Swi6 by 5 peptides (Figure S2F, Table S2). This unbiased analysis suggested that Nsr1 interacts with SBF *in vivo*. To confirm this result, we performed co-immunoprecipitation experiments on extracts of rapamycin-treated cells expressing MYC-tagged *NSR1* or *WHI5* alleles from their endogenous promoters or from an untagged control strain (Figure 4A). Nsr1^{MYC}, Whi5^{MYC}, Swi4 and Swi6 were each immunoprecipated and then blotted with antibodies against each protein. The specific association of Nsr1^{MYC} with both Swi4 and Swi6 resembled that of Whi5^{MYC} suggesting that Nsr1 may directly interact with SBF under physiological conditions.

To determine if the interactions between Nsr1 and SBF were indeed direct, we carried out *in vitro* binding assays with purified recombinant proteins. We titrated recombinant ^{FLAG}Swi4-Swi6 and ^{FLAG}Mbp1-Swi6 complexes produced in baculovirus-infected insect cells (12) against recombinant ^{GST}Nsr1 immobilized on GSH-Sepharose resin. Swi4 and Swi6 were both captured with ^{GST}Nsr1 across the titration series whereas control GSH-Sepharose resin did not bind either protein (Figure 4B). In contrast, ^{GST}Nsr1 did not detectably interact with the ^{FLAG}Mbp1-Swi6 complex under the conditions tested, suggesting that specificity for Nsr1 is determined by the DNA binding subunit and not the common Swi6 subunit. These results demonstrated that endogenous Nsr1 interacts directly and specifically with the Swi4-Swi6 complex, and that no additional factors are needed for this interaction to occur.

Nsr1 binds to SBF-regulated promoters in vivo

We next assessed the presence of Nsr1^{13MYC} at the SBF-regulated promoters of *CLN2* and *PCL1* by chromatin immunoprecipitation (ChIP). For both genes, we specifically detected SCB-containing promoter sequences by PCR in cross-linked MYC immune complexes purified from cells that expressed Nsr1^{13MYC} from the endogenous *NSR1* locus (Figure 4C). The enrichment of *PCL1* and *CLN2* sequences only upon rapamycin-induced Nsr1 expression further demonstrated that Nsr1 specifically binds SBF-regulated G1/S promoter DNA (Figure 4C).

Nsr1 binding to chromatin should reduce the protein mobility in the nucleus. To test this

hypothesis, we assessed the dynamics of Nsr1-GFP in cells grown in nitrogen-limited media using Raster Image Correlation Spectroscopy (RICS). RICS exploits the hidden time structure of imaging scans, in which adjacent pixels are imaged a few microseconds apart, to quantify the diffusional properties of fluorescent molecules (41-43). Intensity correlations between pixels shifted along the direction of scanning (horizontal correlations), and along the orthogonal direction (vertical correlations), are averaged over multiple scans. Horizontal and vertical correlations that decay with increasing pixel shift are characteristic of the dynamical properties on 10-100 μs and 5-50 ms timescales respectively. We found that the vertical RICS correlations of nuclear Nsr1-GFP signal decreased on a slower timescale than either free nuclear GFP or cytosolic Nsr1-GFP signal (Figure 4D). Fitted diffusion coefficients were correspondingly lower for nuclear Nsr1 compared to free nuclear GFP or cytosolic Nsr1, and were closer to that of DNA-bound Swi6-GFP (Figure 4D). This result indicated that Nsr1 associates with a slowly-moving nuclear component, most likely chromatin.

The size epistasis between *whi5Δ* and *GAL1-NSR1* prompted us to ask whether Nsr1 might reduce the association Whi5 with SBF and/or chromatin. However, ChIP analysis of $Whi5^{HA}$ at the *CLN2* and *PCL1* promoters revealed that $Whi5^{HA}$-promoter interactions were not reduced in the presence of overexpressed Nsr1 (Figure S3A). In addition, *GAL1-NSR1* cells had wild-type levels of Whi5 as determined by sN&B quantification (Figure S3B) and Nsr1 did not alter $Whi5^{HA}$ association with Swi4 or Swi6 in co-immunoprecipitation experiments (Figure S3C). Nsr1 and Whi5 also did not compete for SBF binding in *in vitro* binding assays with recombinant proteins (Figure S3D). Together, these results obtained using different *in vivo, in vitro*, biochemical and imaging-based approaches suggested that Nsr1 binds SBF at G1/S promoters *in vivo*, but that this binding does not alter Whi5 interactions with SBF or promoter DNA.

Nsr1 confers transcriptional activity that can rescue G1/S-transcription deficient mutants

We next hypothesized that Nsr1 might directly contribute to G1/S transcriptional activation. To test this hypothesis, we expressed a Nsr1-Gal4 DNA binding domain fusion protein (GAL4-DBD-NSR1) in cells where the *HIS3* auxotrophic marker is under the control of the *GAL1* promoter. We

used the *GAL4-DBD* alone and *GAL4-DBD* fused to an irrelevant human gene (*UBE2G2*) that potently transactivates as negative and positive controls, respectively. Full length *NSR1* but not its conserved C-terminus was able to activate transcription of the *HIS3* reporter and thereby allow cell growth in medium lacking histidine (Figure 5A).

Given the apparent transactivation activity of Nsr1, we then tested whether Nsr1 overexpression could suppress the growth defects of mutants in which G1/S transcription was impaired. We first tested a *mbp1Δ swi4-ts* double mutant (44). The growth of *GAL1-NSR1 mbp1Δ swi4-ts* cells was improved with respect to the *mbp1Δ swi4-ts* control at a semi-permissive temperature of 30° in galactose medium, but not in other media or at the permissive temperature (Figure 5B; Figure S4B). As a further test, we examined suppression in strains that expressed $WHI5^{12A}$ and $SWI6^{SA4}$ alleles in which all Cdc28 consensus sites are mutated, a combination that abrogates Cln-Cdc28 mediated relief of SBF inhibition by Whi5 (12, 14). Overexpression of *NSR1* also partially rescued the growth defect of this strain (Figure 5C). These results suggested that Nsr1 provides an alternative mechanism of Start activation by augmenting G1/S transcription irrespective of Whi5 inhibition.

Nsr1 contributes to bypass Whi5 inhibition of SBF

To test whether physiological levels of Nsr1 targeted to SBF are sufficient to promote Start activation, we constructed a strain expressing a Whi5-Nsr1-GFP fusion protein from the endogenous *WHI5* promoter. In rich nitrogen medium, i.e., when endogenous Nsr1 is not expressed, the chimeric protein was expressed and had the expected molecular mass (Figure S5A). The Whi5-Nsr1-GFP chimera retained the localization pattern of endogenous Whi5, with about 30-35% of pre-Start cells showing a prominent nuclear signal (Figures 6A; Figure S5B). Cells expressing Whi5-Nsr1-GFP were almost as small as *whi5Δ* cells (Figure 6B), and as small as cells that expressed *GAL1-NSR1* in galactose medium (Figure 6C). The small size phenotype conferred by the Whi5-Nsr1-GFP expression was not due to the presence of the GFP tag since size distributions of strains expressing untagged versus GFP-tagged Whi5 were indistinguishable (Figure S5C). Moreover, cells expressing the chimeric protein grew at the same rate as WT and *whi5Δ* strains (Figure S5D).

As a reduction of Whi5 dosage in the Whi5-Nsr1-GFP fusion context could in principle explain the small size of this strain, we used sN&B to compare the nuclear concentrations of Whi5 in the WT and the Nsr1-fusion contexts. Whi5 levels in WT cells were 110-130 nM, consistent with those determined previously (30). The Whi5-Nsr1-GFP chimera was present at a slightly lower concentration, 80-100nM (Figure 6A), close to endogenous Nsr1 nuclear levels in nitrogen-limited media (60-80nM, see Figure 2C). This slight decrease in Whi5 abundance was unlikely to explain the small size of cells expressing Whi5-Nsr1-GFP since cell size is not strongly sensitive to *WHI5* gene dosage (45). We confirmed that hemizygous *WHI5/whi5Δ* diploid cells were only marginally smaller than WT diploid cells (Figure S5E) and *WHI5* overexpression only causes a 20-30% increase in mode size (Figure 3C), in agreement with previous results (45). Consistently, our previously published Start model (30) also predicted that downregulating Whi5 levels from 120nM to 85nM should not affect the critical size at Start (Figure S5F).

Finally, we predicted that the Whi5-Nsr1 fusion should be sufficient to rescue the lethal Start arrest of a *cln3Δ bck2Δ* strain. We crossed a *cln3Δ* strain bearing the integrated *WHI5-NSR1-GFP* allele to a *bck2Δ* strain and analyzed growth of dissected tetrads on selective media to identify spore genotypes (Figure 6D). We recovered many viable *cln3Δ bck2Δ WHI5-NSR1-GFP* triple mutant spore clones but did not recover any viable *cln3Δ bck2Δ WHI5* double mutant clones (Figure 6D). As expected, no viable *cln3Δ bck2Δ* spore clones were obtained from a control cross of a *cln3Δ WHI5-GFP* and a *bck2Δ* strain (Figure 6D). These results supported the model in which Nsr1 bypasses Whi5 inhibition by directly conferring transactivation activity to the inhibited SBF complex.

Discussion

On the premise that additional genes may activate Start under suboptimal nutrient conditions, we screened for genes that can circumvent the Start arrest caused by loss of *CLN3* and *BCK2* function. We discovered that *NSR1* overexpression efficiently bypasses the lethality of a *cln3Δ bck2Δ* strain and activates Start in wild type cells; that Nsr1 associates with SBF at G1/S promoter DNA; that *NSR1* overexpression can genetically suppress defects in SBF function; and that Nsr1 is itself a transcriptional activator. Our data suggest a model whereby nitrogen

depletion or TORC1 inhibition promote NSR1 expression, likely via the TORC1-regulated transcription factor Gln3 (46, 47). Subsequent Nsr1 binding to SBF yields a direct recruitment of the transcriptional machinery such that Nsr1 bypasses Whi5-mediated inhibition of SBF (Figure 6E). In effect, Nsr1 acts as a nutrient-dependent parallel input into SBF. As we have not been able to identify nutrient conditions in which loss of NSR1 causes a Start delay, we infer that NSR1 function is strongly buffered by other Start activators.

This model allows interpretation of some previous *YLR053c/NSR1* genetic interactions uncovered in high-throughput studies(48). Deletion of *NSR1* slightly aggravates the growth defect of a Ess1 prolyl isomerase mutant which in turn exhibits negative genetic interactions with deletions of *SWI6* or *SWI4* (49). Although the latter interactions suggested a possible role of Ess1 in Swi6/Whi5 nuclear import, we did not observe mis-localization of Swi4, Swi6 or Whi5 in *GAL1-NSR1* and *nsr1Δ* strains. With respect to interactions with the transcriptional machinery, *NSR1* overexpression exacerbates the defect caused by deletion of *CTK1*, the catalytic subunit of RNA Pol II C-terminal domain (CTD) kinase I (50). In contrast, *NSR1* deletion shows a positive genetic interaction with the RNA Pol II CTD-associated phosphatase, FCP1, which negatively regulates transcription (51). *NSR1* overexpression also subtly increases chromosomal instability (52), which might result from premature Start activation (53). These interactions with transcriptional regulators are consistent with our proposed model for Nsr1 function in G1/S transcription activation.

Nsr1 is a member of a newly described class of genetic elements variously called proto-genes, neo-ORFs, smORFS, small ORF encoded peptides, or microproteins (36, 54-62). Computational predictions and ribosomal footprinting first identified hundreds of short species-specific translated peptides from non-genic sequences in yeast (36). Subsequent approaches have yielded a plethora of microproteins encoded by smORFs in various species (54-57). Documented functions for microproteins include phagocytosis (58), mitochondrial function (59), actin-based motility (60) and mitotic chromosome segregation (61). D*e novo* appearance of short proto-genes coupled with rapid evolution may form a dynamic reservoir for genetic innovation and diversification (36). Notably, fast evolving genes often have complex expression patterns

compared to highly conserved genes and tend to be enriched for transcription-associated functions (63). As illustrated by the example of *NSR1*, transcription activation may be a particularly facile route for proto-genes to quickly acquire important regulatory functions that optimize fitness under specific conditions.

Methods

Yeast strains construction and culture

All strains were isogenic with the S288C (BY4741) background (Table S1). Standard molecular genetics methods were employed for genomic integration of C-terminal tagging cassettes (64). Standard media were used for yeast growth: rich (XY: 2% peptone, 1% yeast extract, 0.01% adenine, 0.02% tryptophan); synthetic complete (SC: 0.2% amino acids, 0.5% ammonium sulphate, 0.17% yeast nitrogen base); or nitrogen-poor (0.17% YNB supplemented with 0.4% proline add histidine, leucine, methionine and uracil to complement auxotrophies as needed). Carbon sources were added to 2% w/v as indicated. Unless otherwise specified, cells were grown to saturation in SC+2% glucose and diluted 1 in 5000 in fresh medium for 16-18h growth prior to experiments. These conditions ensured homeostatic growth in log-phase at the time of experiment at a culture density of 2-5 10^6 cells/mL. For strains bearing constructs expressed under the inducible *GAL1* promoter, the pre-growth stage was performed in SC+2% raffinose, and galactose induction was performed as indicated. Cell size distributions were acquired using a Beckman Z2 Coulter Counter. Growth curves were acquired using a Tecan Sunrise shaker-reader.

SGA screen

A *cln3Δ bck2Δ GAL1-WHI5* strain was mated to an array of 5280 *GAL1-ORF* fusion strains (34). Following haploid selection, strains were scored for growth on selection medium containing 2% galactose. Three replicates of this screen were performed. For the third replicate, expression of the *GAL4* transcription factor was increased in case it was limiting for expression of *WHI5*, the ORFs, or *GAL* genes required for growth in the presence of galactose at the sole carbon source. For this purpose, *GAL4* was placed under the control of strong ADH1 promoter in a *cln3::LEU2*

bck2::NAT^R whi5::Kan^R-pGAL1-WHI5 can1d mfa1::MFA1pr-spHIS5+ GAL4p::HphRpADH1-GAL4 query strain. Screen hits were validated by transformation of the *GAL1-GST-ORF* construct directly into the *cln3Δ bck2Δ GAL1-WHI5* query strain. The *YLR053c* hit was also confirmed by tetrad analysis.

Chromatin Immunoprecipitation

Cells were grown in XY with 2% raffinose, induced with 2% galactose for 6 h to an OD600 ≤0.5 and fixed with 1% formaldehyde. Whole-cell extracts from 50 mL of culture were prepared by glass bead lysis, sonicated to shear chromatin DNA into fragments, and incubated with the appropriate antibody coupled to magnetic beads (Dynabeads PanMouse IgG). Immunoprecipitated DNA was washed, de-crosslinked, purified, and analyzed by quantitative real-time PCR. DNA reactions with appropriate oligonucleotides were set-up with SYBR Green PCR Master Mix (Applied Biosystems) and carried out on an ABI 7500 Fast Real-Time PCR System. Enrichment at the *CLN2* or *PCL1* locus was determined after normalization against values obtained from input samples using *SYP1* as the reference gene.

Immunoprecipitation and immunoblot analysis

Protein extracts were prepared in lysis buffer (10mM HEPES-KOH pH 7.9, 50mM KCl, 1.5mM MgCl2, 1mm EDTA, 0.5mM DTT, 50mM NaF, 50mM sodium pyrophosphate, 1mM Na3VO4 and Roche protease inhibitor cocktail) by glass bead lysis. Immunoaffinity purifications were carried out at 4°C for 2 h with indicated antibodies, beads were washed 3 times with wash buffer (10mM Tris-Cl pH7.9, 0.1% Triton X-100, 0.5mM DTT, 0.2mM EDTA, 10% glycerol, 150mM NaCl), and resuspended in SDS sample buffer. Proteins were resolved by SDS-PAGE, transferred onto nitrocellulose membrane and immunoblotted with anti-HA, anti-Swi4 or anti-Swi6 (gift from Brenda Andrews), anti-GST, anti-Sic1 or 9E10 monoclonal antibodies, followed by detection with HRP-conjugated secondary antibody (12, 65). For phosphatase assays, immunoprecipitates were incubated at 37°C for 1 h in either buffer or 600U of lambda (λ)–phosphatase with or without phosphatase inhibitors prior to SDS-PAGE and immunoblot detection.

In vitro binding assays

Recombinant GST-Nsr1 fusion protein was affinity purified with GSH-Sepharose 4B (Amersham Biosciences) in 50 mM HEPES-NaOH, pH 7.5, 150 mM NaCl, 5 mM EDTA, 5mM NaF, 0.1% NP-40, 10% glycerol, supplemented with 1mM PMSF. Recombinant SBF or MBF complex was purified with anti-FLAG resin (M2, Sigma) from insect cells co-infected with FlagSwi6/Swi6 or FlagMbp1/Swi6 baculovirus, in buffer supplemented with complete protease inhibitor cocktail (Roche), and then eluted with excess FLAG peptide (12). Binding reactions were incubated at 4°C for 1h with rotation. Washed samples were resolved on SDS-PAGE gel followed by immunoblotting with anti-FLAG (M2, Sigma) and anti-Swi6. For competition assays, Clb5-Cdc28 complexes were isolated from yeast cultures using anti-Clb5 antibodies. SBF-GST-Nsr1 and SBF-HA-Whi5 complexes were pre-formed in solution and immobilized on anti-FLAG and anti-HA resin, respectively, incubated with GST-Nsr1, HA-Whi5 or both Clb5/Cdc28 and GST-Nsr1, washed and analyzed as described above.

Immunoprecipitation and mass spectrometry analysis

Cell pellets from untagged and Nsr1^{13MYC} strains from 100 mL of culture at OD_{600} = 1 were lysed in standard lysis buffer (50mM Tris-HCl pH8.0, 150mM KCl, 100mM NaF, 10% glycerol, 0.1% tween-20, 1mM tungstate, 1mM DTT, 10mM AEBSF, 10 mM pepstatin A, 10 mM E-64) (43) supplemented with protease inhibitors using a N_2(l) freezer mill. Lysates (0.5 mL) were incubated for 1 h with 5 μL of anti-MYC antibody (Gentex) followed by 1 h incubation with an additional 50 μL of GammaBind plus Sepharose beads (GE Healthcare) to capture protein complexes. After multiple washes, samples were separated on BioRad precast gels and the entire gel lane was cut for each sample (CAPCA core facility, https://capca.iric.ca/; see Supplemental Methods). Gel samples were destained, alkylated and digested with trypsin for 8 h at 37°C and peptides extracted in 90% ACN. Peptides were separated on a home-made C18 column connected to Q-Exactive HF Biopharma with a 56 min gradient of 0% to 30% acetonitrile in 0.2% formic acid. Each full MS spectrum of extracted peptides was acquired at a resolution of 120,000, followed by acquisition of 15 tandem-MS (MS-MS) spectra on the most abundant multiply charged precursor ions by collision-induced dissociation (HCD). Data were processed using PEAKS X (Bioinformatics

Solutions, Waterloo, ON) and the UniProt yeast database. Variable selected posttranslational modifications were carbamidomethyl (C), oxidation (M), deamidation (NQ), acetyl (N-ter) and phosphorylation (STY). Control untagged and Nsr1^{13MYC} data were analyzed with Scaffold 4.8.9 at a false-discovery rate (FDR) of 1% for at least 2 peptides with a likelihood of at least 99%.

High-content imaging

High-content images were acquired on an OPERA high-throughput confocal microscope (PerkinElmer) equipped with a 60x water objective. Pixel resolution was 220 nm at 2*2 binning. 200 µL of culture were directly transferred to a Greiner Screenstar glass-bottom 96 well imaging plate, and imaged within 30-45 minutes. GFP was excited with a 488nm laser (800 ms exposure for endogenously tagged proteins, 320 ms for overexpressed proteins), and detected using a 520/35 nm band-pass filter. For *WHI5-GFP* and *WHI5-NSR1-GFP* strains, pre-Start G1 phase cells were identified by nuclear localization of the GFP signal, as computed using a custom image-analysis script written in MATLAB (MathWorks). The script masks individual cells using threshold-based detection of the autofluorescence background, and determines the fraction of individual cells that display a pre-Start nuclear localization of the GFP signal.

sN&B and RICS fluorescence fluctuation microscopy

Live cells in log-phase were imaged on a ISS Alba sN&B system comprised of an inverted confocal Nikon Eclipse microscope equipped with a 100x water objective, a Fianium Whitelase continuous white laser with 488 nm emission filters and single photon APD detectors, as described previously (30). In brief, 1.5 mL of cell culture was pelleted for 2 min at 3000 rpm, resuspended in ~100 µL of culture supernatant and 3 µL deposited on a pre-set 65 µL drop of SC+2% glucose+2% agar gel medium on a circular glass coverslip (#1, VWR) that was encircled by an adhesive silicon ring. After 4 min drying time, a ConcanavalinA-coated (Sigma, 2mg/mL) coverslip was gently pressed on top of the agarose to seal the pad against the adhesive silicon ring. Sealed pads were clamped in an AttoFluor chamber (Molecular Probes) and immediately imaged for no more than 1.5 h. Unless otherwise specified, the culture growth medium was re-used to make the imaging pads in order to prevent inadvertent nutrient up- or down-shifts. For this purpose, 1 mL of cell culture

was pelleted at 15000 rpm for 1min and 500 μL of the supernatant was mixed with 10 mg of agarose and warmed for 1-2 min at 98°C to melt the agar, followed by application to a coverslip. For sN&B experiments in the presence of rapamycin, growth medium containing 100 nM rapamycin was also used to prepare the pad. To mitigate possible degradation of rapamycin during the pad preparation, an additional 100 nM of rapamycin was added to the pre-warmed agar mix just before making the pad.

sN&B imaging was performed using 20 raster scans of the same 30 μm-wide Fields of View (FOVs) of 256 pixels (pixel size 117 nm), using an excitation power of 1-2 μW at 488 nm wavelength and a 64 μs pixel dwell time. sN&B images shown in the figures are projections of the 20 raster scans. Protein concentrations were extracted from sN&B data using custom analysis software (30). RICS imaging was performed in a similar fashion to sN&B imaging but different parameters were used to improve correlation curves (pixel size of 48.8 nm, 50 frames, 20 μs pixel dwell time) as described previously (43). RICS vertical correlations for individual FOVs were fitted to single mode-free diffusion models using the SimFCS analysis software. FOVs of poor-quality fit were discarded from diffusion coefficients plots.

Bioinformatics

The sequences of orthologs of *YLR053c* were obtained from the Fungal Orthogroups website. For *S. paradoxus* and *S. mikatae*, where no ORF was predicted at the expected locus, the *YLR053c* sequence was searched against whole genome assemblies using TBLASTN 2.2.27 to predict orthologs. The synteny of the regions in *K. waltii* and *S. cerevisae* was confirmed based on Orthogroups orthology assignments of the upstream (47.17997 and *IES3*) and downstream (47.18006 and *OSW2*) genes and the fact that each of these assignments were supported by highly significant Blast e-values. Alignments were generated using ClustalO 1.2.0 and displayed using the MView online tool.

Mathematical model of Start

Whisker and box plots for model predictions of the critical size at Start were obtained using the mathematical model and the data processing procedure described previously (30). For each plot,

50 individual cells bearing variable Whi5 concentrations randomly picked in the 100-140 nM (for the Whi5-GFP strain) and 65-105nM (for the Whi5-Nsr1-GFP strain) ranges were simulated, and plots generated in Excel using standard statistics of the distributions of critical size values for each strain.

Data Availability

The mass spectrometry proteomics data have been deposited to the ProteomeXchange Consortium via the PRIDE (66) partner repository with the dataset identifier PXD018681 and DOI 10.6019/PXD018681.

Acknowledgments

We thank Marc Angeli for technical assistance with SGA screens and Brenda Andrews for providing reagents and strains. This work was supported by a grant from the Canadian Institutes of Health Research (FDN-167277) to M.T., a Genomics Technology Platform award from Genome Canada to M.T. and P.T., a Genomics Applications Partnership Program award from Genome Canada and Genome Quebec to P.T., an Institute for Data Valorisation (IVADO) postdoctoral fellowship to J.C.-H., and a Canada Research Chair in Systems and Synthetic Biology to M. T.

Competing interests

The authors declare no competing interests.

Author contributions

Conceptualization: J.S., S.T., M.T.; Data Curation: S.T., J.C-H.; Formal Analysis: S.T., J.C-H.; Funding Acquisition: M.T.; Investigation and Validation: S.T., J.S., Y.T., J.T., S.M., D.B.; Methodology: S.T., J.S., J.T., S.M., C.A.R., M.T.; Project Administration and Supervision: S.T., M.T.; Resources: S.T., J.S., Y.T., J.T., S.M., D.B.; Software: S.T., J.C-H.; Visualization: S.T., J.S., Y.T; Writing – Original Draft Preparation: S.T., J.S., D.B.; Writing – Review & Editing: S.T., Y.T., J.C-H., C.A.R., M.T.

References

1. Broach JR. Nutritional control of growth and development in yeast. Genetics. 2012;192(1):73-105.
2. Johnston GC, Pringle JR, Hartwell LH. Coordination of growth with cell division in the yeast Saccharomyces cerevisiae. Exp Cell Res. 1977;105(1):79-98.
3. Jorgensen P, Tyers M. How cells coordinate growth and division. Curr Biol. 2004;14(23):R1014-27.
4. Lowndes NF, Johnson AL, Breeden L, Johnston LH. SWI6 protein is required for transcription of the periodically expressed DNA synthesis genes in budding yeast. Nature. 1992;357(6378):505-8.
5. Primig M, Sockanathan S, Auer H, Nasmyth K. Anatomy of a transcription factor important for the start of the cell cycle in Saccharomyces cerevisiae. Nature. 1992;358(6387):593-7.
6. Koch C, Moll T, Neuberg M, Ahorn H, Nasmyth K. A role for the transcription factors Mbp1 and Swi4 in progression from G1 to S phase. Science. 1993;261(5128):1551-7.
7. Iyer VR, Horak CE, Scafe CS, Botstein D, Snyder M, Brown PO. Genomic binding sites of the yeast cell-cycle transcription factors SBF and MBF. Nature. 2001;409(6819):533-8.
8. Lee TI, Rinaldi NJ, Robert F, Odom DT, Bar-Joseph Z, Gerber GK, et al. Transcriptional regulatory networks in Saccharomyces cerevisiae. Science. 2002;298(5594):799-804.
9. Simon I, Barnett J, Hannett N, Harbison CT, Rinaldi NJ, Volkert TL, et al. Serial regulation of transcriptional regulators in the yeast cell cycle. Cell. 2001;106(6):697-708.
10. Ferrezuelo F, Colomina N, Futcher B, Aldea M. The transcriptional network activated by Cln3 cyclin at the G1-to-S transition of the yeast cell cycle. Genome Biol. 2010;11(6):R67.
11. Jorgensen P, Nishikawa JL, Breitkreutz BJ, Tyers M. Systematic identification of pathways that couple cell growth and division in yeast. Science. 2002;297(5580):395-400.
12. Costanzo M, Nishikawa JL, Tang X, Millman JS, Schub O, Breitkreuz K, et al. CDK activity antagonizes Whi5, an inhibitor of G1/S transcription in yeast. Cell. 2004;117(7):899-913.
13. de Bruin RA, McDonald WH, Kalashnikova TI, Yates J, 3rd, Wittenberg C. Cln3 activates G1-specific transcription via phosphorylation of the SBF bound repressor Whi5. Cell. 2004;117(7):887-98.
14. Wagner MV, Smolka MB, de Bruin RA, Zhou H, Wittenberg C, Dowdy SF. Whi5 regulation by site specific CDK-phosphorylation in Saccharomyces cerevisiae. PLoS One. 2009;4(1):e4300.
15. Skotheim JM, Di Talia S, Siggia ED, Cross FR. Positive feedback of G1 cyclins ensures coherent cell cycle entry. Nature. 2008;454(7202):291-6.
16. Tyers M, Tokiwa G, Futcher B. Comparison of the Saccharomyces cerevisiae G1 cyclins: Cln3 may be an upstream activator of Cln1, Cln2 and other cyclins. EMBO J. 1993;12(5):1955-68.
17. McInerny CJ, Partridge JF, Mikesell GE, Creemer DP, Breeden LL. A novel Mcm1-dependent element in the SWI4, CLN3, CDC6, and CDC47 promoters activates M/G1-specific transcription. Genes Dev. 1997;11(10):1277-88.
18. Nash R, Tokiwa G, Anand S, Erickson K, Futcher AB. The WHI1+ gene of Saccharomyces cerevisiae tethers cell division to cell size and is a cyclin homolog. EMBO J. 1988;7(13):4335-46.
19. Liu X, Wang X, Yang X, Liu S, Jiang L, Qu Y, et al. Reliable cell cycle commitment in budding yeast is ensured by signal integration. Elife. 2015;4.
20. Litsios A, Huberts D, Terpstra HM, Guerra P, Schmidt A, Buczak K, et al. Differential scaling between G1 protein production and cell size dynamics promotes commitment to the cell division cycle in budding yeast. Nat Cell Biol. 2019;21(11):1382-92.
21. Wijnen H, Futcher B. Genetic analysis of the shared role of CLN3 and BCK2 at the G(1)-S transition in Saccharomyces cerevisiae. Genetics. 1999;153(3):1131-43.
22. Bastajian N, Friesen H, Andrews BJ. Bck2 acts through the MADS box protein Mcm1 to activate cell-cycle-regulated genes in budding yeast. PLoS Genet. 2013;9(5):e1003507.
23. Tokiwa G, Tyers M, Volpe T, Futcher B. Inhibition of G1 cyclin activity by the Ras/cAMP pathway in yeast. Nature. 1994;371(6495):342-5.
24. Flick K, Chapman-Shimshoni D, Stuart D, Guaderrama M, Wittenberg C. Regulation of cell size by glucose is exerted via repression of the CLN1 promoter. Mol Cell Biol. 1998;18(5):2492-501.

25. Jorgensen P, Rupes I, Sharom JR, Schneper L, Broach JR, Tyers M. A dynamic transcriptional network communicates growth potential to ribosome synthesis and critical cell size. Genes Dev. 2004;18(20):2491-505.
26. Lempiainen H, Uotila A, Urban J, Dohnal I, Ammerer G, Loewith R, et al. Sfp1 interaction with TORC1 and Mrs6 reveals feedback regulation on TOR signaling. Mol Cell. 2009;33(6):704-16.
27. Singh J, Tyers M. A Rab escort protein integrates the secretion system with TOR signaling and ribosome biogenesis. Genes Dev. 2009;23(16):1944-58.
28. Urban J, Soulard A, Huber A, Lippman S, Mukhopadhyay D, Deloche O, et al. Sch9 is a major target of TORC1 in Saccharomyces cerevisiae. Mol Cell. 2007;26(5):663-74.
29. Talarek N, Gueydon E, Schwob E. Homeostatic control of START through negative feedback between Cln3-Cdk1 and Rim15/Greatwall kinase in budding yeast. Elife. 2017;6.
30. Dorsey S, Tollis S, Cheng J, Black L, Notley S, Tyers M, et al. G1/S Transcription Factor Copy Number Is a Growth-Dependent Determinant of Cell Cycle Commitment in Yeast. Cell Syst. 2018;6(5):539-54 e11.
31. Epstein CB, Cross FR. Genes that can bypass the CLN requirement for Saccharomyces cerevisiae cell cycle START. Mol Cell Biol. 1994;14(3):2041-7.
32. Di Como CJ, Chang H, Arndt KT. Activation of CLN1 and CLN2 G1 cyclin gene expression by BCK2. Mol Cell Biol. 1995;15(4):1835-46.
33. Tong AH, Evangelista M, Parsons AB, Xu H, Bader GD, Page N, et al. Systematic genetic analysis with ordered arrays of yeast deletion mutants. Science. 2001;294(5550):2364-8.
34. Sopko R, Huang D, Preston N, Chua G, Papp B, Kafadar K, et al. Mapping pathways and phenotypes by systematic gene overexpression. Mol Cell. 2006;21(3):319-30.
35. Zhu H, Bilgin M, Bangham R, Hall D, Casamayor A, Bertone P, et al. Global analysis of protein activities using proteome chips. Science. 2001;293(5537):2101-5.
36. Carvunis AR, Rolland T, Wapinski I, Calderwood MA, Yildirim MA, Simonis N, et al. Proto-genes and de novo gene birth. Nature. 2012;487(7407):370-4.
37. Digman MA, Dalal R, Horwitz AF, Gratton E. Mapping the number of molecules and brightness in the laser scanning microscope. Biophys J. 2008;94(6):2320-32.
38. Balleza E, Kim JM, Cluzel P. Systematic characterization of maturation time of fluorescent proteins in living cells. Nat Methods. 2018;15(1):47-51.
39. Daran-Lapujade P, Jansen ML, Daran JM, van Gulik W, de Winde JH, Pronk JT. Role of transcriptional regulation in controlling fluxes in central carbon metabolism of Saccharomyces cerevisiae. A chemostat culture study. J Biol Chem. 2004;279(10):9125-38.
40. Boer VM, de Winde JH, Pronk JT, Piper MD. The genome-wide transcriptional responses of Saccharomyces cerevisiae grown on glucose in aerobic chemostat cultures limited for carbon, nitrogen, phosphorus, or sulfur. J Biol Chem. 2003;278(5):3265-74.
41. Brown CM, Dalal RB, Hebert B, Digman MA, Horwitz AR, Gratton E. Raster image correlation spectroscopy (RICS) for measuring fast protein dynamics and concentrations with a commercial laser scanning confocal microscope. J Microsc. 2008;229(Pt 1):78-91.
42. Digman MA, Wiseman PW, Horwitz AR, Gratton E. Detecting protein complexes in living cells from laser scanning confocal image sequences by the cross correlation raster image spectroscopy method. Biophys J. 2009;96(2):707-16.
43. Thattikota Y, Tollis S, Palou R, Vinet J, Tyers M, D'Amours D. Cdc48/VCP Promotes Chromosome Morphogenesis by Releasing Condensin from Self-Entrapment in Chromatin. Mol Cell. 2018;69(4):664-76 e5.
44. Gray JV, Ogas JP, Kamada Y, Stone M, Levin DE, Herskowitz I. A role for the Pkc1 MAP kinase pathway of Saccharomyces cerevisiae in bud emergence and identification of a putative upstream regulator. EMBO J. 1997;16(16):4924-37.

45. Adames NR, Schuck PL, Chen KC, Murali TM, Tyson JJ, Peccoud J. Experimental testing of a new integrated model of the budding yeast Start transition. Mol Biol Cell. 2015;26(22):3966-84.
46. Beck T, Hall MN. The TOR signalling pathway controls nuclear localization of nutrient-regulated transcription factors. Nature. 1999;402(6762):689-92.
47. Minehart PL, Magasanik B. Sequence and expression of GLN3, a positive nitrogen regulatory gene of Saccharomyces cerevisiae encoding a protein with a putative zinc finger DNA-binding domain. Mol Cell Biol. 1991;11(12):6216-28.
48. Oughtred R, Stark C, Breitkreutz BJ, Rust J, Boucher L, Chang C, et al. The BioGRID interaction database: 2019 update. Nucleic Acids Res. 2019;47(D1):D529-D41.
49. Atencio D, Barnes C, Duncan TM, Willis IM, Hanes SD. The yeast Ess1 prolyl isomerase controls Swi6 and Whi5 nuclear localization. G3 (Bethesda). 2014;4(3):523-37.
50. Sharifpoor S, van Dyk D, Costanzo M, Baryshnikova A, Friesen H, Douglas AC, et al. Functional wiring of the yeast kinome revealed by global analysis of genetic network motifs. Genome Res. 2012;22(4):791-801.
51. Costanzo M, VanderSluis B, Koch EN, Baryshnikova A, Pons C, Tan G, et al. A global genetic interaction network maps a wiring diagram of cellular function. Science. 2016;353(6306).
52. Frumkin JP, Patra BN, Sevold A, Ganguly K, Patel C, Yoon S, et al. The interplay between chromosome stability and cell cycle control explored through gene-gene interaction and computational simulation. Nucleic Acids Res. 2016;44(17):8073-85.
53. Tanaka S, Diffley JF. Deregulated G1-cyclin expression induces genomic instability by preventing efficient pre-RC formation. Genes Dev. 2002;16(20):2639-49.
54. Ma J, Ward CC, Jungreis I, Slavoff SA, Schwaid AG, Neveu J, et al. Discovery of human sORF-encoded polypeptides (SEPs) in cell lines and tissue. J Proteome Res. 2014;13(3):1757-65.
55. Ladoukakis E, Pereira V, Magny EG, Eyre-Walker A, Couso JP. Hundreds of putatively functional small open reading frames in Drosophila. Genome Biol. 2011;12(11):R118.
56. Kastenmayer JP, Ni L, Chu A, Kitchen LE, Au WC, Yang H, et al. Functional genomics of genes with small open reading frames (sORFs) in S. cerevisiae. Genome Res. 2006;16(3):365-73.
57. Ma J, Diedrich JK, Jungreis I, Donaldson C, Vaughan J, Kellis M, et al. Improved Identification and Analysis of Small Open Reading Frame Encoded Polypeptides. Anal Chem. 2016;88(7):3967-75.
58. Pueyo JI, Magny EG, Sampson CJ, Amin U, Evans IR, Bishop SA, et al. Hemotin, a Regulator of Phagocytosis Encoded by a Small ORF and Conserved across Metazoans. PLoS Biol. 2016;14(3):e1002395.
59. Gong Z, Tasset I, Diaz A, Anguiano J, Tas E, Cui L, et al. Humanin is an endogenous activator of chaperone-mediated autophagy. J Cell Biol. 2018;217(2):635-47.
60. Polycarpou-Schwarz M, Gross M, Mestdagh P, Schott J, Grund SE, Hildenbrand C, et al. The cancer-associated microprotein CASIMO1 controls cell proliferation and interacts with squalene epoxidase modulating lipid droplet formation. Oncogene. 2018;37(34):4750-68.
61. Li JM, Li Y, Elledge SJ. Genetic analysis of the kinetochore DASH complex reveals an antagonistic relationship with the ras/protein kinase A pathway and a novel subunit required for Ask1 association. Mol Cell Biol. 2005;25(2):767-78.
62. Saghatelian A, Couso JP. Discovery and characterization of smORF-encoded bioactive polypeptides. Nat Chem Biol. 2015;11(12):909-16.
63. Coulombe-Huntington J, Xia Y. Network Centrality Analysis in Fungi Reveals Complex Regulation of Lost and Gained Genes. PLoS One. 2017;12(1):e0169459.
64. Fink GR. Guide to Yeast Genetics and Molecular and Cell Biology. Guthrie C, editor. San Francisco, California: Academic Press, Elsevier; 2002. 12 p.
65. Tang X, Orlicky S, Mittag T, Csizmok V, Pawson T, Forman-Kay JD, et al. Composite low affinity interactions dictate recognition of the cyclin-dependent kinase inhibitor Sic1 by the SCFCdc4 ubiquitin ligase. Proc Natl Acad Sci U S A. 2012;109(9):3287-92.

66. Perez-Riverol Y, Csordas A, Bai J, Bernal-Llinares M, Hewapathirana S, Kundu DJ, et al. The PRIDE database and related tools and resources in 2019: improving support for quantification data. Nucleic Acids Res. 2019;47(D1):D442-D50.

Figure and Table Legends

Figure 1: A genome-wide screen identifies YLR053c/NSR1 as a dosage suppressor of *cln3Δ bck2Δ* lethality

(A) Schematic of SGA genetic screen for dosage suppressors of *cln3Δ bck2Δ* lethality. (**B)** Representative screen plate scored for growth on galactose medium. Red box, *GAL1-YLR053c*. (**C)** Comparison of growth at 30°C for the indicated strains streaked onto either glucose or galactose medium. **(D)** Chromosomal region around *YLR053c/NSR1* on Chr. XII and translated 108 amino acid (12.7 kDa) protein sequence. **(E)** Ylr053c/Nsr1 protein sequence in *S. cerevisiae* (top) aligned with sequences of other yeast species. Conservation of a KKXNPFYVPSXVVREMV motif at the C-terminal across evolutionary distant species is indicated by a red bar.

Table 1: Other dosage suppressors of the *cln3Δ bck2Δ* lethality

Genes identified in our three SGA-based genome-wide screens as dosage suppressors of the *cln3Δ bck2Δ* lethality. Genes are grouped according to whether they were identified in the 3 screens (first group, 12 genes), in 2 screens out of 3 (second group, 22 genes) or only once (third group, 63 genes). *YLR053c/NSR1* belongs to the first group and is indicated in red.

Figure 2: Nitrogen deprivation and rapamycin treatment induce cell cycle-regulated Nsr1 expression

(A) sN&B images of untagged and *NSR1-GFP* strains. Cells were grown and imaged in SC+2%glucose with or without 100nM rapamycin, SC+2%raffinose or YNB+0.4%proline+2%glucose+HIS, LEU, MET, URA (referred to as YNB pro glu), as indicated. Scale bar is 10 μm. The same intensity scale was used for all conditions. **(B)** Abundance of MYC-tagged Nsr1 in various nutrient conditions as determined by immunoblot of anti-MYC immune complexes. IgG indicates antibody light chain. **(C)** Absolute Nsr1 concentration in single cells grown and imaged in YNB pro glu as a function of cell size, as determined by sN&B. Blue and orange dots represent individual cells from two different experiments. The typical size range of cells at the G1/S transition (800-1000 pixels, corresponding to 27-38 fL) is indicated. Cell-averaged total Nsr1 concentration (top) and nuclear concentration where Nsr1 nuclear

localization was evident (bottom) are shown. Infrequent small cells with high Nsr1 levels had high autofluorescence and no nuclear localization of the signal. **(D)** High-content confocal image of log-phase Nsr1-GFP cells grown and imaged in YNB pro glu.

Figure 3: *NSR1* is genetically upstream of SBF

Cell size distributions were determined for the indicated genetic combinations. (A) Effect of *NSR1* overexpression alone. (B) Interaction of *NSR1* overexpression with *cln3Δ* and *bck2Δ* mutations. (C) Interaction of *NSR1* overexpression and *nsr1Δ* mutation with *WHI5* overexpression and *whi5Δ* mutation. (D) Interaction of *NSR1* overexpression with *swi4Δ* and *swi6Δ* mutations. (E) Interaction of *NSR1* overexpression with *swi4-ts* mutation. Strains were transformed with *GAL1-NSR1*, *GAL1-WHI5* plasmids or empty vector controls as indicated. Strains bearing galactose-regulated constructs and associated controls were induced for 6 h in SC+2% galactose before size determination. WT plots in panels B, C and D (left, middle) represent the same measurement.

Figure 4: Nsr1 binds to SBF and SBF-regulated promoter DNA

(A) Nsr1^{13MYC}, Swi4, or Swi6 complexes were immunoprecipitated from a rapamycin-treated Nsr1^{13MYC} strain and interacting proteins assessed by immunoblot. Co-immunoprecipitation of Whi5^{13MYC} with Swi4 and Swi6 served as a positive control. **(B)** Recombinant ^{GST}Nsr1 immobilized on GSH-Sepharose resin was incubated with increasing concentrations of purified SBF (^{Flag}Swi4-Swi6) or MBF (^{Flag}Mbp1-Swi6). Bound proteins were analysed by SDS-PAGE electrophoresis and immunoblotting with anti-Swi6 and anti-Flag antibodies as indicated. GSH-Sepharose resin alone served as a negative control. **(C)** Anti-MYC chromatin immunoprecipitations from wild-type untagged control and *nsr1::NSR1^{13MYC}* strains either untreated or treated with 200 ng/mL of rapamycin for 2 h were probed for the presence of *CLN2* and *PCL1* promoter DNA sequences by real time PCR. **(D)** Top panel: RICS vertical correlations from Nsr1-GFP cells grown in YNB pro glu as a function of the pixel shift for total and cytosolic Nsr1-GFP pools. RICS correlation for free GFP was used as a control for unconstrained diffusion. Data points show correlation averages over N fields of view (FOV, N=25 for nuclear Nsr1, N=7 for cytosolic Nsr1, N=12 for free GFP). Each FOV contained 1-5 cells. Error bars represent the standard error on the mean. Bottom panel: Scatter

plots of fitted diffusion coefficients from individual FOVs of the same strains. Data from Swi6-GFP FOVs served as a control for constrained diffusion due to a strong interaction with DNA.

Figure 5: Nsr1 transcription function rescues G1/S-transcription deficient mutants

(A) Transactivation of a *HIS3* reporter by fusion of Nsr1 to the Gal4 DNA binding domain (DBD) but not by fusion of the Nsr1 C-terminus. *GAL4-DBD-UBE2G2 and GAL4-DBD* constructs served as positive and negative controls, respectively. Growth curves were determined in -His -Trp medium. **(B)** Serial 5-fold dilutions of *NSR1* and *GAL1-NSR1* strains in the WT, *swi4-ts*, *mbp1Δ* and *mbp1Δswi4-ts* backgrounds were spotted onto SC+2% glucose, SC+2% raffinose and SC+2% galactose, and grown for 5 days at 30°C. **(C)** Serial 5-fold dilutions of WT or *swi6Δ* strains transformed with *GAL1-WHI5*, *GAL1-WHI5*^{12A}, *GAL1-SWI6*^{SA4}, *GAL1-NSR1* or empty control plasmids or combinations thereof as indicated. Cells were spotted on rich medium containing 2% glucose or 2% galactose and grown for 2 days at 30°C.

Figure 6: Nsr1 bypasses Whi5 inhibition of SBF

(A) sN&B microscopy images of Whi5-GFP and Whi5-Nsr1-GFP cells grown in SC+2% glucose. Scale bars are 5 µm. The same intensity scale was used on both images. Fractions of pre-Start G1 cells were computed based on the assessment of nuclear GFP signal in Whi5-GFP cells (N=245) and Whi5-Nsr1-GFP (N=95) cells. Absolute concentrations of Whi5-GFP and Whi5-Nsr1-GFP are shown in the plot. **(B)** Cell size distributions of WT (black), *GAL1-NSR1* (blue), *whi5Δ* (red) and *WHI5-NSR1-GFP* (purple) strains in SC+2% glucose. **(C)** Cell size distributions of WT (black), *GAL1-NSR1* (blue), *whi5Δ* (red) and *WHI5-NSR1-GFP* (purple) strains in SC+2% galactose. **(D)** Genotyping of 10 tetrads from a *cln3Δ WHI5-NSR1-GFP* X *bck2Δ* cross (top) and a *cln3Δ WHI5-GFP* X *bck2Δ* cross (bottom). For each tetrad, spore clone growth was assessed on SD-LEU (indicates *cln3::LEU2*), SC+NAT (indicates *bck2::NAT*^{R}), and SD-HIS (indicates *whi5::WHI5-NSR1-GFP-HIS3* or *whi5::WHI5-GFP-HIS3*). Coloured boxes indicate viable *cln3Δ bck2Δ* spore clones, all of which also contained the *WHI5-NSR1-GFP* construct. **(F)** Simplified schematic for Nsr1-dependent activation of Start. Red lines indicate nitrogen limited conditions. Not all components of the Start machinery are shown. See text for details.

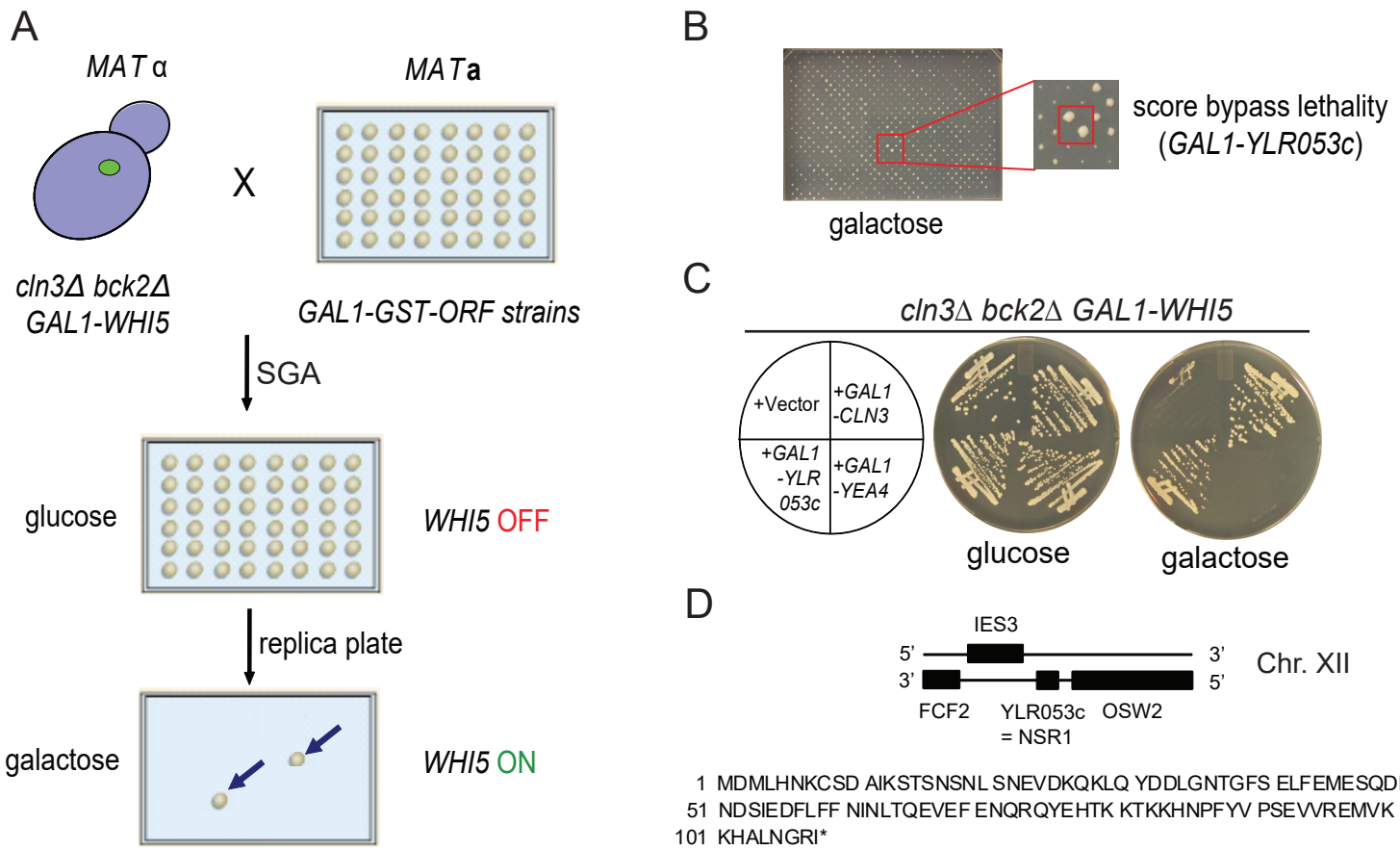

E

```
                          cov    pid   1 [        .         .         .         .         :         .         .         . 80
1 Scas|Scas656.13d     100.0% 100.0%     ------------------------------------------------------------MDLSEYFSTEPVNI
2 Kwal|Kwal47.18002     74.7%  10.4%     MMVFAHTDFEIQDPMLGHLKPFQSPFTEVEQQPRASVEELFGLTGSGAEPDPVIFESELLAPELTLEDL-----------
3 Scer|YLR053C          47.9%  13.1%     -----------MDMLHN--------------KCSDAIKST----------SNSNLSNEVDKQKLQYDDLGNTGFSELFEM
4 Sbay|sbayc672-g32.1   51.4%  12.1%     -MVFLLRSVVLVDMLDD--------------KSSNSVENT----------SDNNWGSEVEKHKQQYEDVEYSMYSEPLEM
  consensus/100%                          ..............................................................Dl...........
  consensus/90%                           ..............................................................Dl...........
  consensus/80%                           ..............................................................Dl...........
  consensus/70%                           ............D.h.s..............pspsulcph..........sss.htsEl.t.c.ph-DLt..h.oE.hph

                          cov    pid  81         .         1         .         .         .         .         :         . 160
1 Scas|Scas656.13d     100.0% 100.0%     LNEESR-------EVSSNTTQHATPEYERIEEELTNLHNLFGIEPDG-TSKRQPKQTRKKSKSNPFYRTPEKVKEYLNRK
2 Kwal|Kwal47.18002     74.7%  10.4%     -REDSNFSFDEELELPVCEL--RELEFEQKAGVETKERQHEQIEGRSRSICSLARPRLPMRKSNPFYFPSRHIKNMISKH
3 Scer|YLR053C          47.9%  13.1%     ESQDNNDSIEDFLFFNINLT--QEVEFENQRQY--------------------EHTKKTKKHNPFYVPSEVVREMVKKH
4 Sbay|sbayc672-g32.1   51.4%  12.1%     EPQDDNENMEDCWYFSMDVG--QELEFERQNQE--------------------GNTTKAKKYNPFYVPSKVVREMVSKA
  consensus/100%                          ..p-sp........hs.s.h..tp.EaEp.tt.....................t.ph.hpK.NPFYhsschl+phlp+t
  consensus/90%                           ..p-sp........hs.s.h..tp.EaEp.tt.....................t.ph.hpK.NPFYhsschl+phlp+t
  consensus/80%                           ..p-sp........hs.s.h..tp.EaEp.tt.....................t.ph.hpK.NPFYhsschl+phlp+t
  consensus/70%                           .spDsN.sh--.h.hshshs..pElEFEpppp.....................cpTpKt+KpNPFYhPSchV+EMlsK+

                          cov    pid 161         .         .         .         2         .         .   ] 224
1 Scas|Scas656.13d     100.0% 100.0%     KSRSTSDALRSLNHNVINNRTKDTENWTKISNEKSRT----PEDSIDQDIDRHSTNQKRKNTHK
2 Kwal|Kwal47.18002     74.7%  10.4%     RQRKNGPKIENE----------TQSQWNSTEDLLVKCSDAKPFLERRQTIG-------------
3 Scer|YLR053C          47.9%  13.1%     ALNGRI-----------------------------------------------------------
4 Sbay|sbayc672-g32.1   51.4%  12.1%     GVEWQSIA--KS----------K------------------------------------------
  consensus/100%                          t.p.p.........................................................
  consensus/90%                           t.p.p.........................................................
  consensus/80%                           t.p.p.........................................................
  consensus/70%                           t.ctpu.t..p...........p.......................................
```

Tollis *et al.* Figure 1

Table 1: Genes whose overexpression rescues *cln3Δ bck2Δ* pGAL1-WHI5 lethality on galactose

Systematic name	Standard name	Gene function (SGD)
Genes identified in 3/3 screens		
YAL039C	CYC3	Cytochrome c heme lyase (holocytochrome c synthase); attaches he
YAL040C	CLN3	G1 cyclin involved in cell cycle progression; activates Cdc28p kinase
YDR133C	YDR133C	Dubious open reading frame; unlikely to encode a functional protein,
YEL004W	YEA4	Uridine diphosphate-N-acetylglucosamine (UDP-GlcNAc) transporte
YLR053C	YLR053C/NSR1	Putative protein of unknown function
YLR294C	YLR294C	Dubious open reading frame; unlikely to encode a functional protein,
YMR199W	CLN1	G1 cyclin involved in regulation of the cell cycle; activates Cdc28p ki
YOR099W	KTR1	Alpha-1,2-mannosyltransferase; involved in O- and N-linked protein
YOR202W	HIS3	Imidazoleglycerol-phosphate dehydratase; catalyzes the sixth step ir
YOR209C	NPT1	Nicotinate phosphoribosyltransferase; acts in the salvage pathway o
YOR250C	CLP1	Component of the cleavage and polyadenylation factor I (CF I); CF 1
YPL082C	MOT1	Essential protein involved in regulation of transcription; removes Spt
Genes identified in 2/3 screens		
YBL062W	YBL062W	Dubious open reading frame; unlikely to encode a functional protein,
YBL067C	UBP13	Ubiquitin-specific protease that cleaves Ub-protein fusions; UBP13 h
YBL071C	YBL071C	Putative protein of unknown function; conserved among S. cerevisia
YCL018W	LEU2	Beta-isopropylmalate dehydrogenase (IMDH); catalyzes the third ste
YCL055W	KAR4	Transcription factor required for response to pheromones; also requ
YCR060W	TAH1	Component of conserved R2TP complex (Rvb1-Rvb2-Tah1-Pih1); F
YDR359C	EAF1	Component of the NuA4 histone acetyltransferase complex; acts as
YGR029W	ERV1	Flavin-linked sulfhydryl oxidase of the mitochondrial IMS; N-terminus
YHR023W	MYO1	Type II myosin heavy chain; required for wild-type cytokinesis and ce
YHR035W	NEL1	Activator of Sar1p GTPase activity; paralog of Sec23 but does not a
YHR039C-A	VMA10	Subunit G of the V1 peripheral membrane domain of V-ATPase; par
YJL007C	YJL007C	Putative protein of unknown function; conserved among S. cerevisia
YJL220W	YJL220W	Dubious open reading frame; unlikely to encode a functional protein,
YJR091C	JSN1	Member of the Puf family of RNA-binding proteins; interacts with mF
YLR245C	CDD1	Cytidine deaminase; catalyzes the modification of cytidine to uridine
YMR125W	STO1	Large subunit of the nuclear mRNA cap-binding protein complex; int
YMR290W-A	YMR290W-A	Dubious open reading frame; unlikely to encode a functional protein,
YNL250W	RAD50	Subunit of MRX complex with Mre11p and Xrs2p; complex is involve
YNR011C	PRP2	RNA-dependent DExD/H-box ATPase; required for activation of spli
YOR285W	RDL1	Thiosulfate sulfurtransferase; contains a rhodanese-like domain; loc
YPL035C	YPL035C	Dubious open reading frame; unlikely to encode a functional protein,
YPL142C	YPL142C	Dubious open reading frame; unlikely to encode a functional protein,
Genes identified in 1/3 screen		
YAL045C	YAL045C	Dubious open reading frame; unlikely to encode a functional protein,
YAR007C	RFA1	Subunit of heterotrimeric Replication Protein A (RPA); RPA is a high
YBL006C	LDB7	Component of the RSC chromatin remodeling complex; interacts wit
YBL044W	YBL044W	Putative protein of unknown function; YBL044W is not an essential p
YBL051C	PIN4	Protein involved in G2/M phase progression and response to DNA d
YBR235W	VHC1	Vacuolar membrane cation-chloride cotransporter (CCC); likely med
YBR278W	DPB3	Third-largest subunit of DNA polymerase II (DNA polymerase epsilo
YCL022C	YCL022C	Dubious open reading frame; unlikely to encode a functional protein,
YCR003W	MRPL32	Mitochondrial ribosomal protein of the large subunit; protein abunda
YCR073C	SSK22	MAP kinase kinase kinase of HOG1 mitogen-activated signaling pat
YCR085W	YCR085W	Putative protein of unknown function; conserved among S. cerevisia
YDL068W	YDL068W	Dubious open reading frame; unlikely to encode a functional protein,
YDL215C	GDH2	NAD(+)-dependent glutamate dehydrogenase; degrades glutamate t
YDR162C	NBP2	Protein involved in the HOG (high osmolarity glycerol) pathway; nega

YDR310C	SUM1	Transcriptional repressor that regulates middle-sporulation genes; re
YDR336W	MRX8	Protein that associates with mitochondrial ribosome; sumoylated unc
YDR393W	SHE9	Protein required for normal mitochondrial morphology; mitochondrial
YDR407C	TRS120	Component of transport protein particle (TRAPP) complex II; TRAPP
YDR420W	HKR1	Mucin family member that functions as an osmosensor in the HOG p
YER010C	YER010C	Bifunctional HMG aldolase/oxaloacetate decarboxylase; requires div
YFR007W	YFH7	Putative kinase with similarity to the PRK/URK/PANK kinase subfam
YGL041C	YGL041C	Dubious open reading frame; unlikely to encode a functional protein,
YGL128C	CWC23	Component of a complex containing Cef1p; putatively involved in pre
YGL168W	HUR1	Protein with a role in DNA repair; mutants show reduced efficiency o
YGR037C	ACB1	Acyl-CoA-binding protein; transports newly synthesized acyl-CoA est
YGR211W	ZPR1	Essential protein with two zinc fingers; present in nucleus of growing
YGR237C	YGR237C	Putative protein of unknown function; green fluorescent protein (GFP
YHR193C	EGD2	Alpha subunit of the nascent polypeptide-associated complex (NAC)
YIL039W	TED1	GPI-glycan remodelase; conserved phosphoesterase domain-contai
YIL052C	RPL34B	Ribosomal 60S subunit protein L34B; homologous to mammalian rib
YIL110W	HPM1	AdoMet-dependent methyltransferase; involved in a novel 3-methylh
YJR023C	YJR023C	Putative protein of unknown function; open reading frame overlaps L
YJR129C	EFM3	S-adenosylmethionine-dependent methyltransferase; seven-beta-str
YJR151C	DAN4	Cell wall mannoprotein; has similarity to Tir1p, Tir2p, Tir3p, and Tir4
YKL066W	YKL066W	Dubious open reading frame; unlikely to encode a functional protein,
YKL147C	YKL147C	Dubious open reading frame; unlikely to encode a functional protein,
YKR012C	YKR012C	Dubious open reading frame; unlikely to encode a functional protein,
YKR094C	RPL40B	Ubiquitin-ribosomal 60S subunit protein L40B fusion protein; cleaved
YLL045C	RPL8B	Ribosomal 60S subunit protein L8B; required for processing of 27SA
YLR044C	PDC1	Major of three pyruvate decarboxylase isozymes; key enzyme in alco
YLR171W	YLR171W	Dubious open reading frame; unlikely to encode a functional protein,
YML094W	GIM5	Subunit of the heterohexameric cochaperone prefoldin complex; pre
YML100W-A	YML100W-A	Putative protein of unknown function; identified by gene-trapping, mi
YML117W	NAB6	Putative RNA-binding protein; associates with mRNAs encoding cell
YMR020W	FMS1	Polyamine oxidase; converts spermine to spermidine, which is requi
YMR094W	CTF13	Subunit of the CBF3 complex; F-box protein of the leucine-rich-repe
YMR130W	DPI35	Putative protein of unknown function; YMR130W is not an essential
YMR304C-A	YMR304C-A	Dubious open reading frame; unlikely to encode a functional protein,
YNL061W	NOP2	rRNA m5C methyltransferase; methylates cytosine at position 2870
YNL115C	YNL115C	Putative protein of unknown function; green fluorescent protein (GFP
YNL251C	NRD1	RNA-binding subunit of Nrd1 complex; complex interacts with exoso
YNL301C	RPL18B	Ribosomal 60S subunit protein L18B; homologous to mammalian rib
YOL013W-A	YOL013W-A	Putative protein of unknown function; identified by SAGE
YOL139C	CDC33	Translation initiation factor eIF4E; mRNA cap binding protein and su
YOL150C	YOL150C	Dubious open reading frame; unlikely to encode a functional protein,
YOL166C	YOL166C	Dubious open reading frame; unlikely to encode a functional protein,
YOR075W	UFE1	t-SNARE protein required for retrograde vesicular traffic; involved in
YOR187W	TUF1	Mitochondrial translation elongation factor Tu (EF-Tu); involved in fu
YOR200W	YOR200W	Dubious open reading frame; unlikely to encode a functional protein,
YPL239W	YAR1	Ankyrin-repeat containing, nucleocytoplasmic shuttling assembly cha
YPL276W	YPL276W	NAD(+)-dependent formate dehydrogenase; may protect cells from
YPR050C	YPR050C	Dubious open reading frame; unlikely to encode a functional protein,
YPR112C	MRD1	Essential conserved small ribosomal subunit (40s) synthesis factor;

A

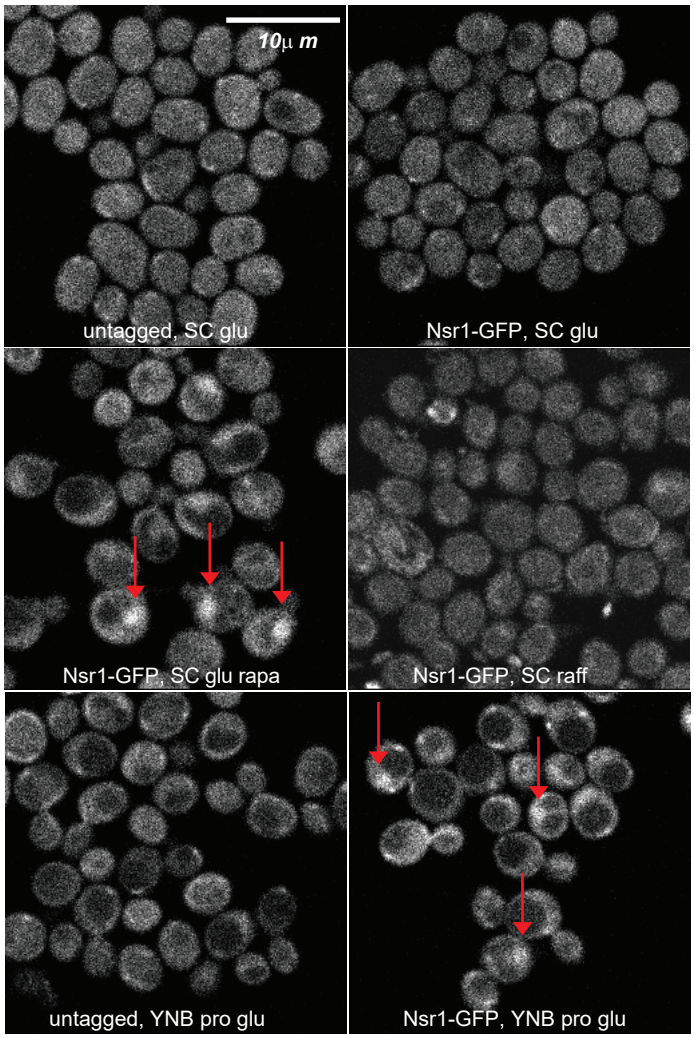

B

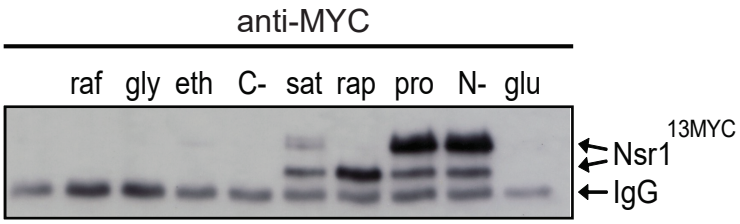

C

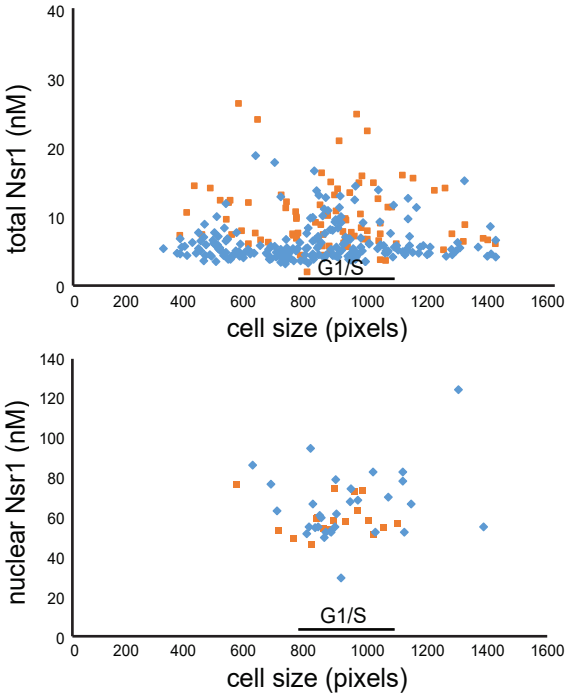

D

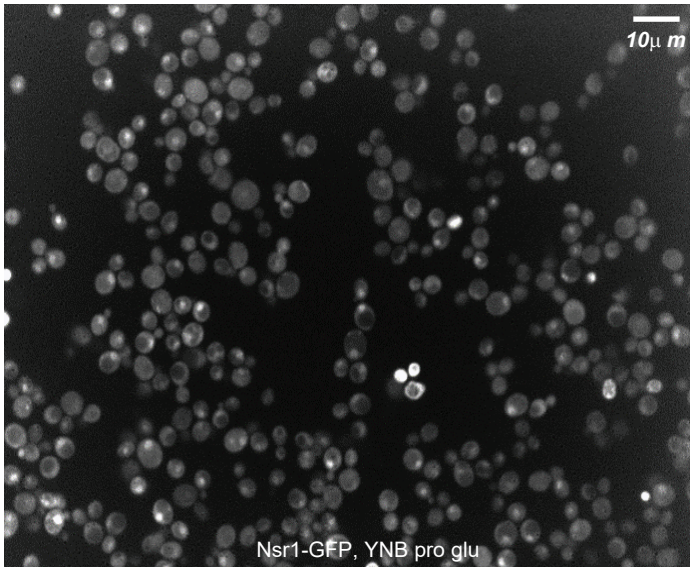

Tollis *et al.* Figure 2

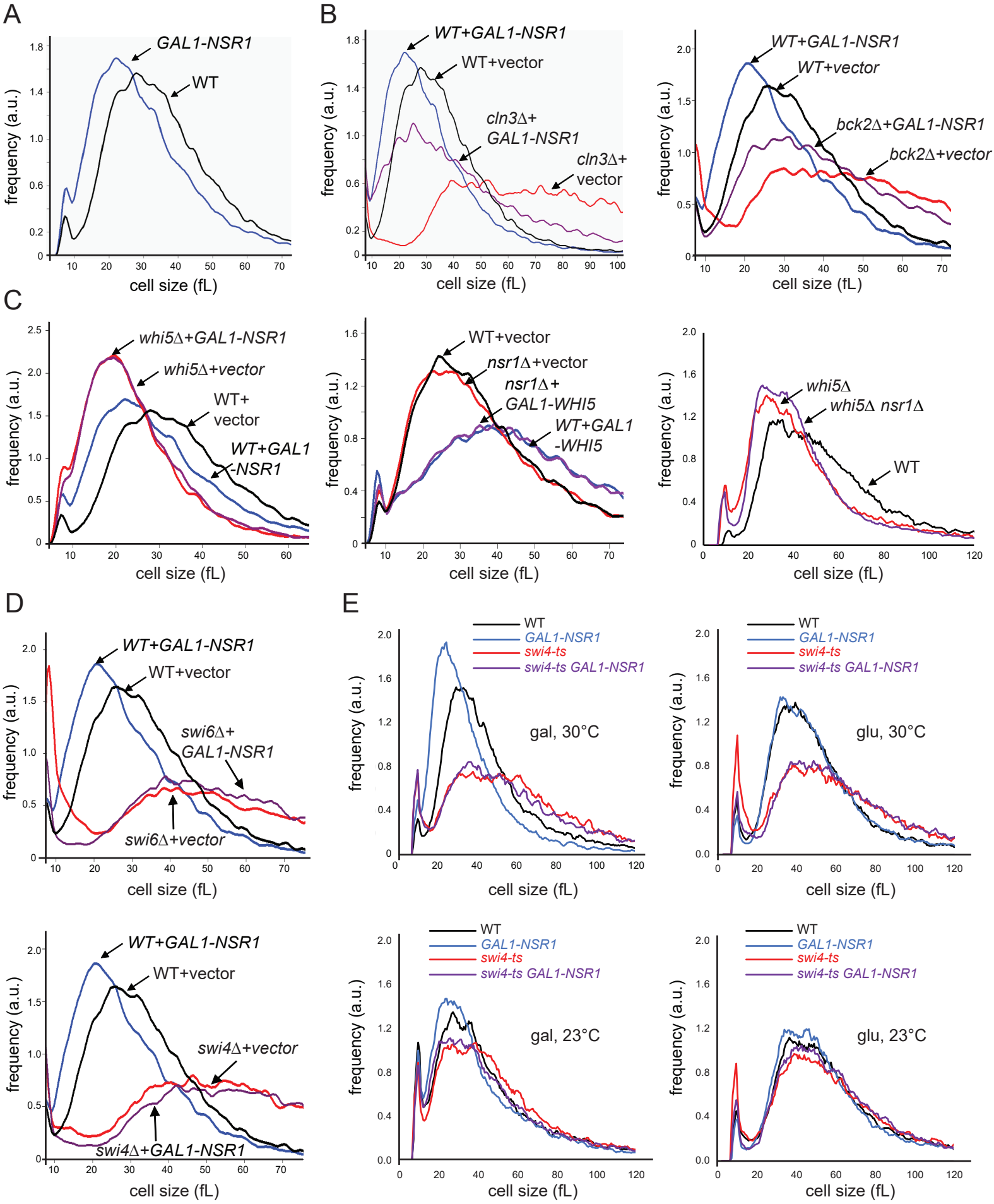

Tollis *et al.* Figure 3

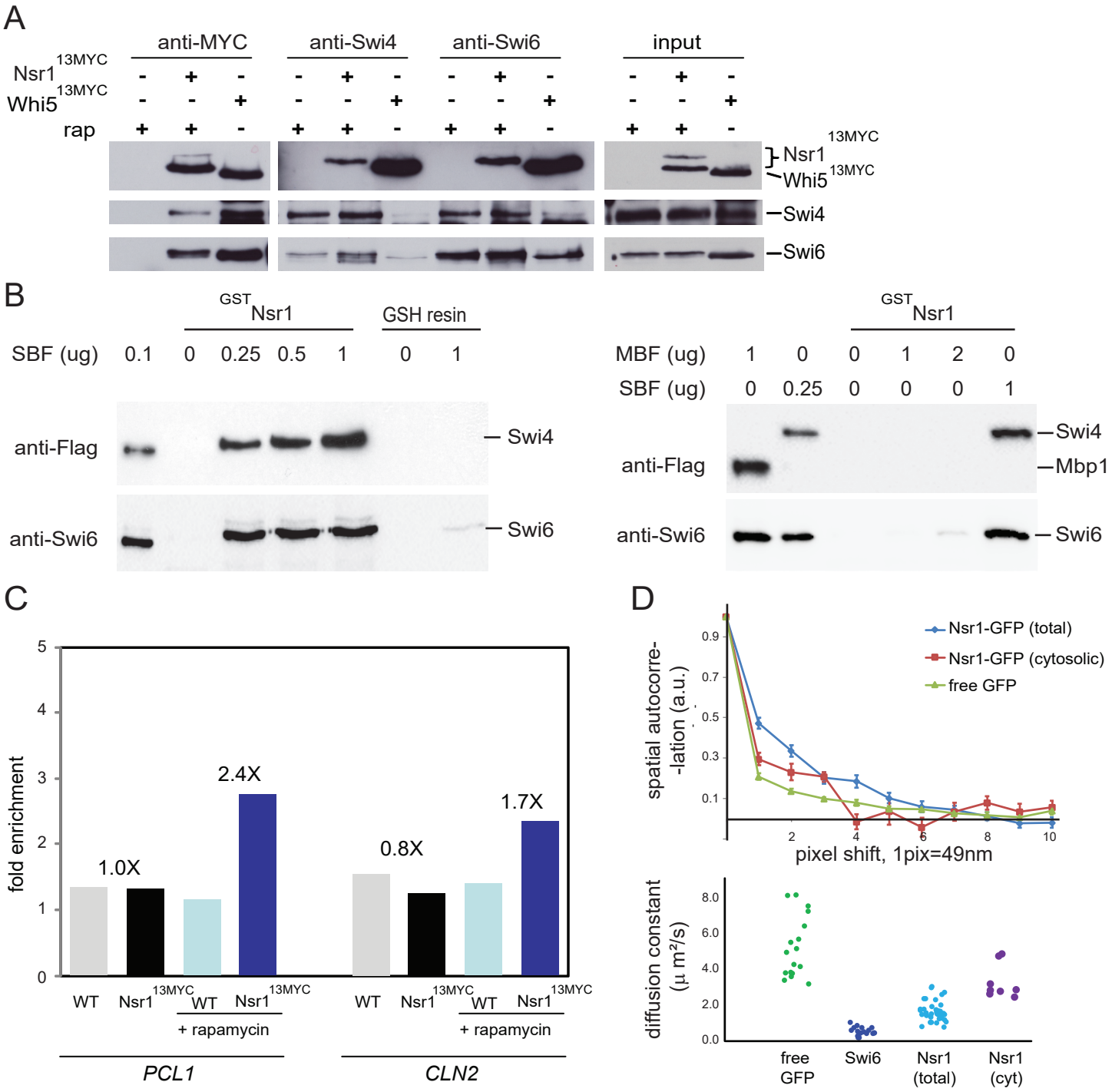

Tollis *et al.* Figure 4

A

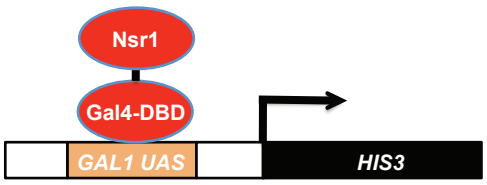

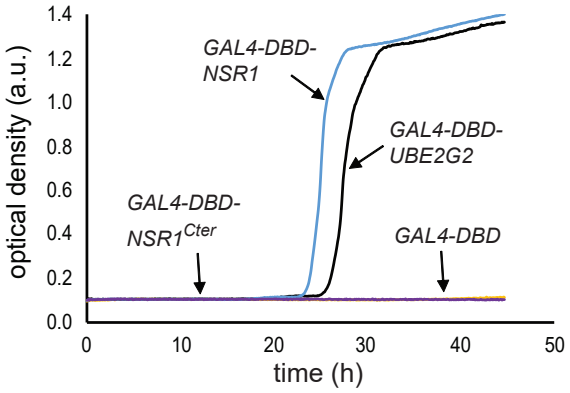

B

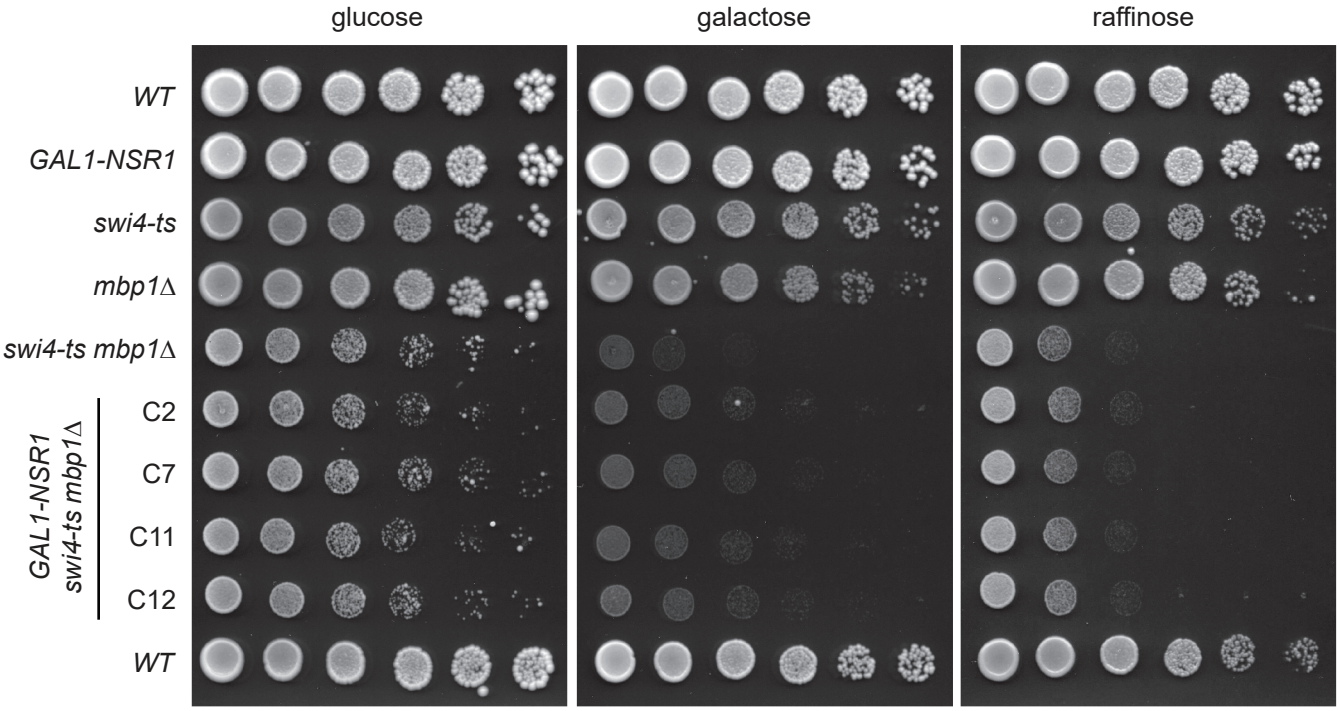

C

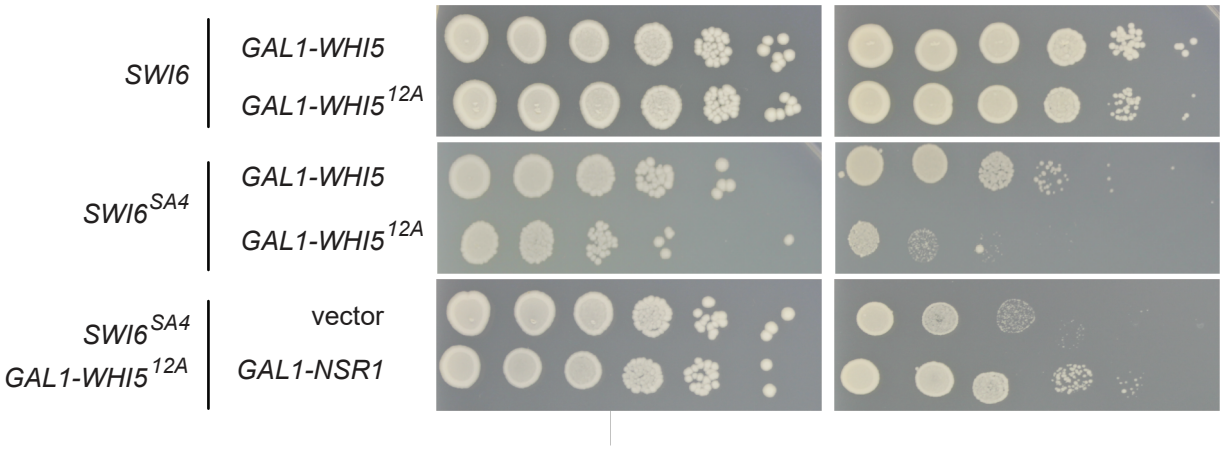

Tollis *et al.* Figure 5

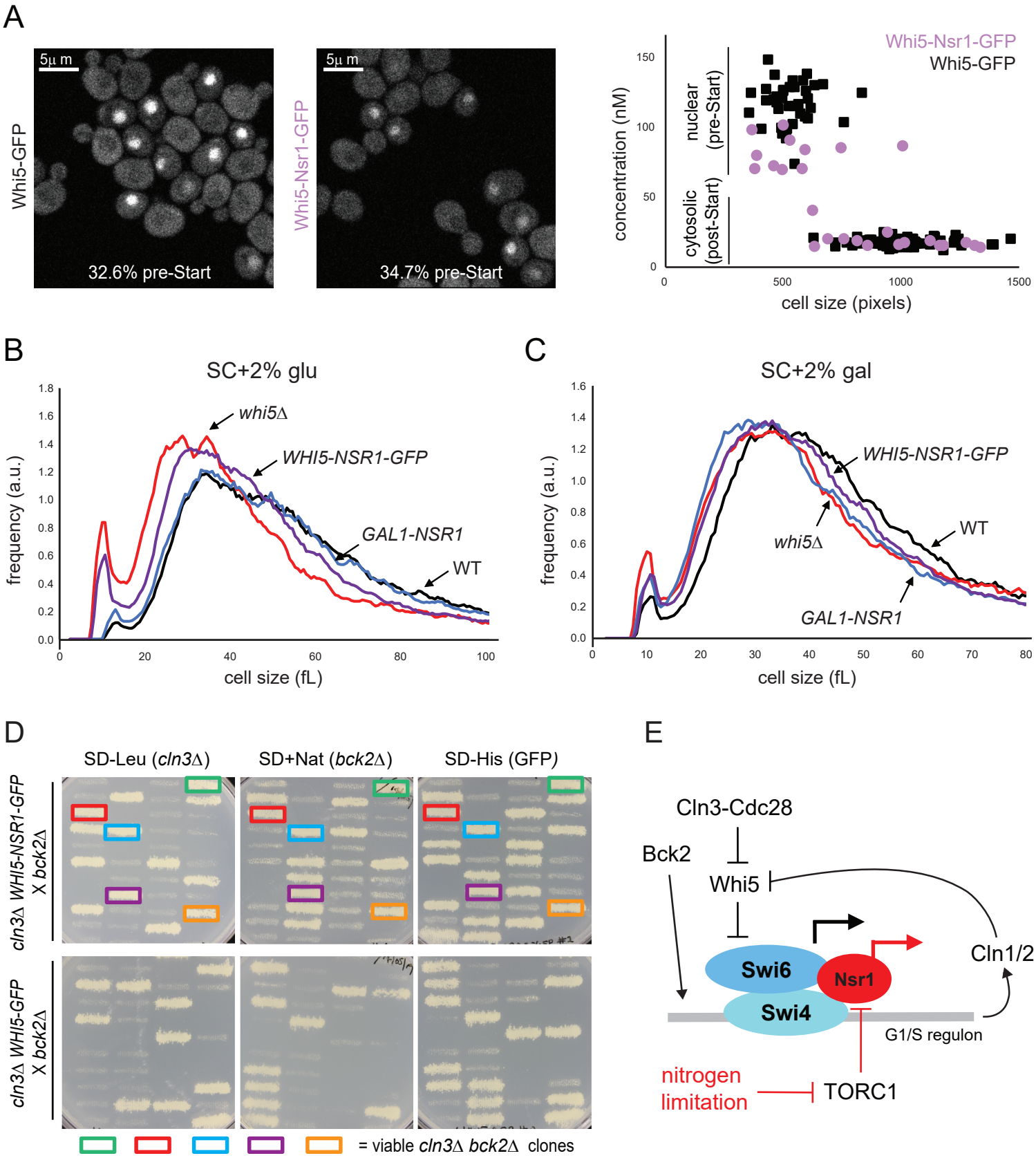

Tollis *et al.* Figure 6

Supplemental Table 1. Yeast strains and plasmids used in this study

Strain name	Strain number	Relevant genotype	MAT	Source
Wild-type (WT) haploid	yMT1448	*his3Δ1 leu2Δ0 met15Δ0 ura3Δ0*	**a**	Winzeler *et al.* 1999
WT diploid	yMT1450	*his3Δ1/his3Δ1 leu2Δ0/leu2Δ0 ura3Δ0/ura3Δ0 MET15/met15Δ0 LYS2/lys2Δ0*	**a**/α	C. Roberts
WHI5/*whi5Δ* diploid, clone 1	yMT5036	*WHI5/whi5::kanMX*	**a**/α	This work
WHI5/*whi5Δ* diploid, clone 2	yMT5037	*WHI5/whi5::kanMX*	**a**/α	This work
WHI5/*whi5Δ* diploid, clone 3	yMT5038	*WHI5/whi5::kanMX*	**a**/α	This work
cln3Δ bck2Δ GAL1-WHI5	yMT4317	*cln3::LEU2, bck2::natMX whi5::kanMX-pGAL1-WHI5, mfa1::MFA1pr-spHIS5+, can1Δ*	α	This work
Nsr1-GFP	yMT5039	*nsr1:: NSR1-mGFPmut3-HIS3MX*	**a**	This work
Nsr1^{13MYC}	yMT4321	*nsr1:: NSR1-13MYC-kanMX*	**a**	This work
Nsr1-WT GFP	yMT5040	*nsr1::NSR1-GFP-natMX*	**-**	This work
nsr1Δ	BY2664	*nsr1::kanMX*	**a**	Giaver *et al.* 2002
sch9as	yMT4237	*sch9::sch9as-natMX*	α	Jorgensen et al. 2004
sch9as nsr1Δ	yMT5041	*sch9::sch9as-natMX nsr1::kanMX*	α	This work
GAL1-NSR1	yMT4323	*lys2Δ0 nsr1::kanMX-pGAL1-NSR1*	**a**	This work
cln3Δ	yMT2125	*cln3::LEU2*	**a**	Jorgensen *et al*. 2002
bck2Δ	BY6163	*bck2::kanMX*	**a**	Giaver *et al.* 2002
swi6Δ	BY4131	*swi6::kanMX*	**a**	Giaver *et al.* 2002
swi4Δ	BY6109	*swi4:: kanMX*	**a**	Giaver *et al.* 2002
swi4-ts	yMT5044	*trp1Δ63 ura3-52 lys2-801a ade2-107o his3Δ200 leu2Δ1 swi4-ts*	α	B. Andrews
swi4-ts GAL1-NSR1	yMT5047	*trp1Δ63 ura3-52 lys2-801a ade2-107o his3Δ200 leu2Δ1 swi4-ts nsr1::kanMX-pGAL1-NSR1*	α	This work
whi5Δ	yMT3249	*whi5::kanMX*	**a**	Costanzo *et al*. 2004
whi5Δ nsr1Δ	yMT5042	*whi5::kanMX nsr1::natMX*	–	This work
Whi5-GFP	yMT5009	*whi5::WHI5-mGFPmut3-HIS3MX*	**a**	Dorsey Tollis *et al.* 2018
GAL1-NSR1 Whi5-GFP	yMT5043	*whi5::WHI5-mGFPmut3-HIS3MX kanMX-pGAL1-NSR1*	–	This work
Swi6-GFP	yMT5006	*Swi6::SWI6-mGFPmut3-HIS3MX*	**a**	Dorsey Tollis *et al.* 2018
Whi5^{13MYC}	yMT3248	*whi5:: WHI5-13MYC-kanMX*	**a**	Costanzo *et al*. 2004
Whi5^{HA}	yMT4325	*whi5:: WHI5-3HA-kanMX*	**a**	This work
GAL1-NSR1 Whi5^{HA}	yMT4320	*nsr1::kanMX-pGAL1-NSR1, whi5:: WHI5-3HA-HIS3MX*	–	This work
Bait strain	AH109	*trp10901, leu2-3, 112, ura3-52, his3-200, gal4Δ, gal80Δ, lys2::GAL1$_{UAS}$-GAL1$_{TATA}$-HIS3, GAL2$_{UAS}$-GAL2$_{TATA}$-ADE2, ura3::MEL1$_{UAS}$-MEL1$_{TATA}$-lacZ*	**a**	Clontech, James *et al.* 1996
WT (Figs 5 and S5, bottom line)	yMT5052	*trp1Δ63 Gal2+ ura3-52 lys2-801a ade2-107o his3Δ200 leu2Δ1*	α	B. Andrews
mbp1Δ	yMT5046	*trp1Δ63 Gal2+ ura3-52 lys2-801a ade2-107o his3Δ200 leu2Δ1 mbp1::TRP1*	α	B. Andrews

Strain name	Strain number	Relevant genotype	MAT	Source
swi4-ts mbp1Δ	yMT5045	*trp1Δ63 Gal2+ ura3-52 lys2-801a ade2-107o his3Δ200 leu2Δ1 swi4-ts mbp1::TRP1*	α	B. Andrews
GAL1-NSR1 swi4-ts mbp1Δ clone C2	yMT5048	*trp1Δ63 Gal2+ ura3-52 lys2-801a ade2-107o his3Δ200 leu2Δ1 swi4-ts mbp1::TRP1 nsr1::kanMX-pGAL1-NSR1*	α	This work
GAL1-NSR1 swi4-ts mbp1Δ clone C7	yMT5049	*trp1Δ63 Gal2+ ura3-52 lys2-801a ade2-107o his3Δ200 leu2Δ1 swi4-ts mbp1::TRP1 nsr1::kanMX-pGAL1-NSR1*	α	This work
GAL1-NSR1 swi4-ts mbp1Δ clone C11	yMT5050	*trp1Δ63 Gal2+ ura3-52 lys2-801a ade2-107o his3Δ200 leu2Δ1 swi4-ts mbp1::TRP1 nsr1::kanMX-pGAL1-NSR1*	α	This work
GAL1-NSR1 swi4-ts mbp1Δ clone C12	yMT5051	*trp1Δ63 Gal2+ ura3-52 lys2-801a ade2-107o his3Δ200 leu2Δ1 swi4-ts mbp1::TRP1 nsr1::kanMX-pGAL1-NSR1*	α	This work
Whi5-Nsr1-GFP	yMT5053	*whi5::WHI5-NSR1-mGFPmut3-HIS3MX*	**a**	This work
bck2Δ	yMT2299	*bck2::natMX*	α	This work
cln3Δ WHI5-NSR1-GFP	yMT5055	*cln3::LEU2 whi5::WHI5-NSR1-mGFPmut3-HIS3MX*	**a**	This work
cln3Δ bck2Δ WHI5-NSR1-GFP clone 1	yMT5057	*cln3::LEU2 bck2::natMX whi5::WHI5-NSR1-mGFPmut3-HIS3MX*	-	This work
cln3Δ bck2Δ WHI5-NSR1-GFP clone 2	yMT5058	*cln3::LEU2 bck2::natMX whi5::WHI5-NSR1-mGFPmut3-HIS3MX*	-	This work
cln3Δ bck2Δ WHI5-NSR1-GFP clone 3	yMT5059	*cln3::LEU2 bck2::natMX whi5::WHI5-NSR1-mGFPmut3-HIS3MX*	-	This work
cln3Δ bck2Δ WHI5-NSR1-GFP clone 4	yMT5060	*cln3::LEU2 bck2::natMX whi5::WHI5-NSR1-mGFPmut3-HIS3MX*	-	This work
cln3Δ bck2Δ WHI5-NSR1-GFP clone 5	yMT5061	*cln3::LEU2 bck2::natMX whi5::WHI5-NSR1-mGFPmut3-HIS3MX*	-	This work
Plasmid name	**Plasmid number**	**Description**		**Source**
pVenus	pMT4642	yEpVenus_URA: URA3 2µ plasmid, TDH3-promoter-driven expression of Venus (YFP)		E. Bilsland, Bilsland *et al.* 2013
pmCherry	pMT4643	yEpGAP-Cherry: URA3 2µ plasmid, TDH3-promoter-driven expression of yEmRFP		N. Dean, Keppler-Ross *et al.* 2008
pGAL1-NSR1	pMT4644	pGAL1-NSR1-HA URA3 CEN plasmid built in the pMT4177 backbone		This work
pGAL1-WHI5	pMT3445	pGAL1-WHI5 HIS3 CEN		Costanzo *et al.* 2004
pGAL4DBD	pMT4645	pGBKT7 cloning vector TRP 2µ		Clontech
pGAL4DBD-UBE2G2	pMT4646	pGBKT7-UBE2G2		This work
pGAL4DBD-NSR1	pMT4647	pGBKT7-NSR1		This work
pGAL4DBD-Cter(NSR1)	pMT4648	pGBKT7-*NSR1*$^{83-99}$		This work
pGAL1-Whi5^{12A}	pMT3455	pGAL1-WHI5^{12A} HIS3 CEN		Costanzo *et al.* 2004
pGAL1-SWI6^{S4A}	pBD1756	SWI6^{S4A} LEU2 2µ plasmid, derived from pBD176		Sidorova *et al.* 1995

* All strains are congenic with yMT1448 (S288C background) unless otherwise indicated.